13 Sensors for Soil, Substrates, and Concrete Based on the MCM100 Microchip

Jos Balendonck[1], Max A. Hilhorst[1], William R. Whalley[2]

[1] Wageningen UR, Agrotechnology and Food Innovations, P.O. Box 17, 6700 AA Wageningen, the Netherlands.
[2] Soil Physics Group, Silsoe Research Institute, Wrest Park, Silsoe, Bedford, MK45 4HS, UK.

13.1 Introduction

Monitoring dielectric properties through impedance measurements to characterize material composition is a commonly known sensing technique and is useful in a broad range of applications. Since the fundamentals of this principle were described [1], many applications based on this technique have been described in the literature. Among them are medical, industrial, agricultural as well as consumer-based applications. They span an enormous broad frequency range, from very low frequencies down to 1 mHz up to the microwave range above 10 GHz.

For research and development, mainly laboratory equipment like the Hewlett Packard impedance analyzers developed in the 1980s are used (Agilent Headquarters, Palo Alto, USA). To compensate for electrode polarization at low frequencies, instruments are available measuring with probes that have three or four electrodes (Solartron Analytical, Farnborough, UK). Recently broadband dielectric spectroscopy analyzers became available that go down to 3 μHz and up to 10 MHz, with good accuracy over an ultra-wide range of 16 decades for resistance and capacitance (Novocontrol GmbH, Hundsangen, Germany). This equipment is suitable for material analysis, since it covers a broad spectral range and even supports on-line temperature control.

In process monitoring as for instance in agriculture, the food industry, and construction engineering, there is an enormous need for low-cost sensors. Dielectric measuring equipment could fulfill this purpose, but the equipment described above is often too expensive and not suited for simple applications. In the 1950s, time domain reflectometry (TDR) became a favorite method to measure material properties with a dielectric method [2]. It is a special form of time domain spectrometry (TDS), while it is operated at a single frequency. In the beginning of the 1980s, cable analyzers were used for this purpose. Since data had to be interpreted visually, they were difficult to control, and they were too expensive to be used as a

simple sensor. Only recently have cheaper TDR sensors become available that make use of advanced digital signal processing [3].

The impedance bridge [4] is one of the oldest applications of the frequency domain (FD) method. Over the years, this method has been applied with varying success. Due to innovations in electronics, stable circuitry has become available which made the use of the FD method at radio frequencies possible [5]. To make simple sensors for on-line process monitoring, the FD method suddenly has potential, especially for water content, but also for other parameters. Over the last two decades a large number of these sensors have come onto the market. Since dielectric properties are obtained at a single frequency, or at a limited number of discrete frequencies, the spectral range of these sensors is limited. We will refer to these techniques as small-band frequency domain spectroscopy (FDS). Sensors based on single frequency measurements are sometimes referred to as frequency domain reflectometry (FDR) sensors or FD sensors. In comparison to other material constituents, water has a high dielectric constant. Therefore, monitoring water content is the most widely spread application for on-line FD sensors. Many of them measure electrical conductivity (EC) as well, since this reflects the total amount of water-dissolved particles. FD sensors are tuned for a specific application. Each one has its own solution for the known problems of electrode polarization, temperature compensation, and the Maxwell–Wagner effect. In general users are not interested in the complex permittivity these sensors measure. They have to relate complex permittivity to the material properties they need, which involves the problem of calibration.

For application in agricultural and for automatic irrigation, numerous FD sensors have been developed to measure water content in soil and other growing media [6–9]. Over the last decade numerous manufacturers have introduced TDR or FD sensors. Examples are the Theta Probe (Delta-T Devices Ltd, Cambridge, UK), the Aquaflex (Streat Instruments, Bromley Christchurch, New Zealand), the TRIME-FM (IMKO Micromodultechnik GmbH, Ettlingen, Germany), and many others [10].

Dielectric measurements have great potential for monitoring moisture in construction materials like cement, sand, or asphalt. Numerous instruments measure moisture based on resistance or capacitance readings [11]. For concrete, this can be for new constructions to measure the hardening process [12], for precautionary purposes to monitor concrete aging [13], or to follow the drying process for curative measures after flooding accidents (TRIME-ES, Micromodultechnik GmbH, Ettlingen Germany).

In food processing, moisture could be measured with the FD method. However, since food texture is complex, the calibration is often a problem. Therefore, near-infrared or microwave technologies have taken over this application. Another promising application here is the monitoring of living cells. Living cells exhibit a very specific dielectric behavior – called the β-relaxation – in the LF and RF spectral range from 30 up to 300 MHz [14]. In this range, cell membranes are short-circuited, and as a result the cell's internal water and protein content can be seen. Many medical and biological sensor applications are based on this phenomenon. To control the fermentation process, in breweries for instance, an instrument is in use

that measures the yeast cell concentration (Aber Instruments Ltd, Aberystwyth, UK). Furthermore the Solartron 1260 (Solartron Analytical, Farnborough, UK) was used to study the behavior of yeast cells when toxic stimuli were applied [15].

All these applications vary in complexity and are more or less built with discrete electronics, which make them either expensive or inaccurate. Some years ago a mixed analog and digital integrated circuit for the measurement of complex impedances became available. It can be used in a frequency range from 10 to 30 MHz. With this microchip, reliable FD sensors can be built [16]. It can also operate at multiple discrete frequencies. So with it, a dielectric spectroscopy sensor with limited frequency range can be built. The small-band discrete spectrum can reveal much more information about the material than a single frequency measurement. In the following sections several applications based on this microchip will be described. They are based upon work from all authors. Much of this work has been published before, and is mentioned in the references. Part of the work was done together with others, who are mentioned in the acknowledgments.

13.2 A Microchip for Impedance Monitoring

In the 1980s, everyone started to use TDR to measure soil water content, working in the higher RF range between 100 and 200 MHz [6, 17]. Some ten years later it was revealed that FD sensors could be calibrated for soil water content in a lower RF range between 10 and 100 MHz as well. Although this calibration appeared to be more sensitive for soil texture, their accuracy was acceptable for practical applications. The FD method was used long before 1980, but the first FD sensors based upon discrete electronics became available around 1990. They measured a frequency shift as the electrical capacitance changed due to variations in water content [5, 7]. The tuning of the electronics was very tedious, and it showed that soon these sensors would only be successful if microchips were used. This would reduce the cost per sensor enormously. However, to ensure high-phase accuracy at the operating frequency (20 MHz), the microchip needed analog circuitry that could work up to 6 GHz. A microprocessor was needed to perform the signal analysis and the calibration task. Therefore, the chip needed an embedded processor or at least a digital interface.

Around 1992 this electronic microchip was designed as an application-specific integrated circuit (ASIC) by using a bipolar CMOS process (SGS-Thomson, Grenoble, France). Prototypes (see Fig. 13.1 left) of this microchip became available in 1994 [16], and shortly thereafter the first prototype FD sensors were built. Positive results were reported [18, 19]. Since only a few external components are needed, it is especially suitable to construct cheap, smart FD sensors to be used for on-line monitoring of water content in agricultural, environmental, and industrial processes. In this section the measuring principle of the microchip is described briefly; more detailed information can be found in other publications [20–22]. In the next sections the application of the chip as a sensor for water content in soils

and substrate materials, pore water conductivity, and strength monitoring for young concrete is described.

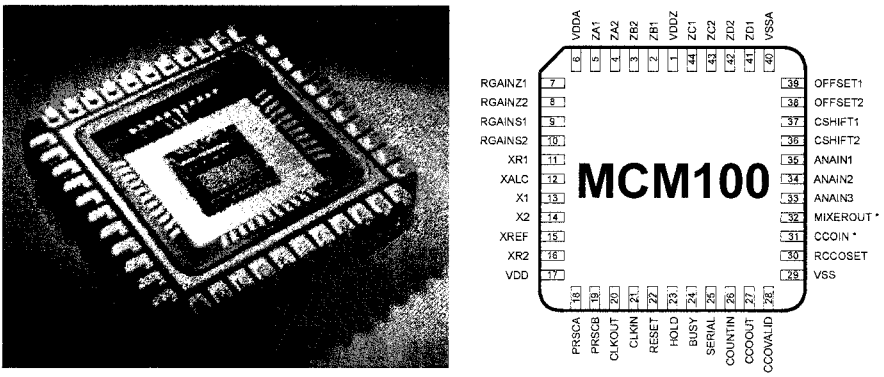

Fig. 13.1. Chip for dielectric measurements in open ceramic package (*left*). Chip pin configuration (*right*)

The microchip, named MCM100, is a vector voltmeter that measures the electric impedance at four differential inputs at a single frequency in the range from 10 to 30 MHz. From the digital data it generates, software can compute permittivity (ε) and conductivity (σ) of the material under test and subsequently volumetric water content. Electrodes can be connected to one of its inputs, via a set of decoupling capacitors that block DC currents through the measured medium, thus preventing electrolysis of the electrodes. Two other inputs can be used to measure a capacitor and resistor with known value as references. Many internal chip errors and even internal and external parasitic components can be compensated for with software. The fourth input can be left open or used for optional purposes (see Fig. 13.1 right).

The microchip has three additional single-ended analog inputs to which external analog or pulse-width-modulated sensors can be connected. Since many physical parameters are temperature dependent, a temperature sensor can be chosen, so measured values can be corrected for temperature. There is a TTL-level serial output that can connect directly to a microprocessor or with a simple RS232-level shifter to a PC or field bus system. Its baud rate can be derived from either the internal or an external clock source. An external prescaler may be used to tune the baud rate and timing of the chip. The output reveals data for the four differential and three analog inputs as well as for internal power and zero. For multiple sensor applications, several chips can be cascaded. This chip operates from a single 5 V power supply using approximately 35 mA. It has an oscillator and reset circuitry on-board, and is commercially available in a standard 44-pin PLCC package.

13.2.1 Operation of the Chip

Internally the chip contains a synchronous detector with a multiplier (×) and low-pass filter (LPF), an analog to digital converter (ADC), a parallel to serial converter (PSC), and timing and controlling logic (see Fig. 13.2). Up to four impedances (Z_A, Z_B, Z_C, Z_D) can be measured at four differential inputs. A sine wave current (i_z) with a frequency determined by an externally connected crystal (f_0), comes from a stabilized oscillator (OSC). It develops a voltage (u_Z) across the unknown impedances that are successively selected by S_1. This voltage is fed to one input of the analog multiplier. A second current (i_{shift}), equivalent to i_z, also comes from the oscillator. Its phase is shifted by respectively 0°, 90°, 180° and 270°, which is controlled by the switches S_2 and S_3. The voltage developed across the phase shifter (u_{shift}) is fed to the other input of the multiplier. The multiplier output (u) consists of a DC and an AC term with frequency $2f_0$. The DC term (U) is found at the output of the LPF. In the case of a 0° and 180° phase shift, U is a measure for the capacitance or inductance of Z_i. In the case of a 90° and 270° phase shift, U is a measure for the conductance of the impedances Z_A to Z_D. The output of the LPF is fed to the ADC and then converted into digital format by the PSC, whose data is outputted at the serial output. In order to compute Z_A to Z_D, this data must be processed further by a processor, which can be connected to the microchip externally.

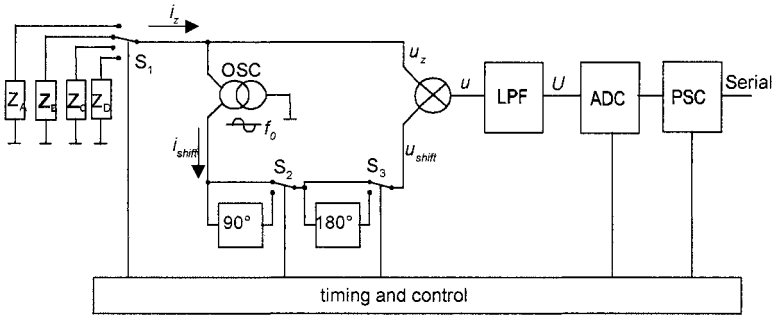

Fig. 13.2. Functional block diagram, showing the internal working of the chip

As long as the microchip is powered, it outputs serial data. Each single measurement (one cycle) involves 22 individual measuring steps. The duration of each step, as well as the baud rate, is dependent on f_0 and the set-up of the internal prescaler (PRSCA, PRSCB in Fig. 13.1, right). For $f_0 = 20$ MHz, typically a baud rate of 1200 Bd and a step time of 100 ms is obtained. There are 16 steps for the four impedances $Z_{A,B,C,D}$ at all four quadrants of the complex plane. Six other steps are used for the three analog inputs of which one is used for temperature and two for internal zero reference. To be able to compensate for a possible warming up of the chip during a measurement cycle, temperature is measured at the beginning and end of the measuring cycle. During every step the microchip outputs a 6-byte

serial ASCII pattern that reflects the step identifier (A, B, ..., U, V) followed by the relative measured value, a five-digit BCD code in the range from 0 to 99999 (see Table 13.1). The serial data is sent as one package containing in total 134 characters starting with character "@" and ending with character "↔". In between these characters, there are the 22 packages belonging to the measuring steps.

Table 13.1. Overview of measuring steps for each measurement cycle

Step	Identifier, value	Comments
Start	@	No measurement
01	Annnnn	Analog input 3
02	Bnnnnn	Offset at beginning
03	Cnnnnn	Analog input 1
04–07	Dnnnnn-Gnnnnn	input Z_A:$U_{0°,90°,180°,270°}$
08–11	Hnnnnn-Knnnnn	input Z_B:$U_{0°,90°,180°,270°}$
12–15	Lnnnnn-Onnnnn	Input Z_C:$U_{0°,90°,180°,270°}$
16–19	Pnnnnn-Snnnnn	Input Z_D:$U_{0°,90°,180°,270°}$
20	Tnnnnn	Analog input 2
21	Unnnnn	Offset at end
22	Vnnnnn	Analog input 3
Stop	↔	No measurement

To build a sensor, only the microchip and a few extra components are needed (see Fig. 13.3). It needs a crystal (XTAL) for the internal clock, an operational amplifier (MAX480) for offset compensation, a reference resistor R_{ref} and a capacitor C_{ref}, two resistors for automatic gain control (R_1 and R_2), and (if needed) an external prescaler to set the baud rate. A set of measuring rods can be connected via two DC-blocking capacitors. As a temperature sensor, a common temperature dependent resistor (NTC), or an active element like the AD590 (Analog Devices) or the SMT160-30 (Smartec, Breda, the Netherlands), can be used. To test the working of the chip a prototype sensor was built. All electronics including the microchip, but excluding a microprocessor and memory, were placed on a printed circuit board (see Fig. 13.4).

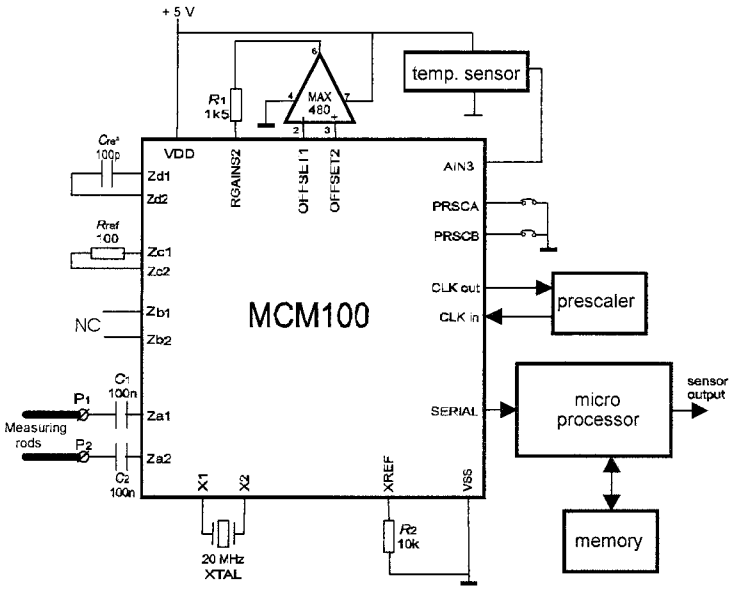

Fig. 13.3. Simplified schematic of sensor electronics (input $Zb_{1,2}$ is left open)

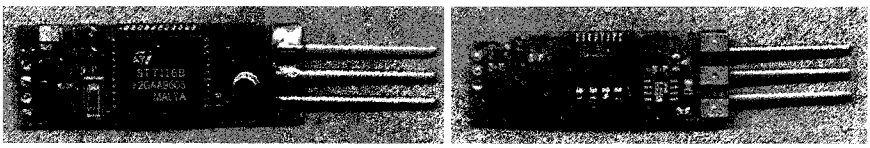

Fig. 13.4. Front side (*left*) of mounted PCB (20×55 mm) with chip, clock crystal, temperature sensor, and three measurement rods (25 mm). Back side (*right*) of PCB with prescaler and offset amplifier

13.2.2 Calibration Procedure and Computation of Dielectric Properties

Besides the unknown impedances $Z_{A,B,C,D}$, parasitic elements like electrodes, inputs, and internal chip circuitry contribute to the total measured impedance. The sensor must therefore be calibrated to measure the complex impedance properly. A simplified four-element model can be used for this. Although it is an approximation for a lumped model transmission line, this model has proven to be adequate for practical applications. It consists of a series inductor (L_s) and resistance (R_s) to model the electrical path length of the electrodes and a parallel capacitor (C_p) and resistor (R_p) that model the input circuitry of the chip (see Fig. 13.5). The values for L_s, R_s, C_p, and R_p are typical for each sensor and need to be obtained

through calibration. The known external reference components (R_{ref} and C_{ref}) are used to compute C_p and R_p. Internal chip offsets are compensated for by subtracting two 180° phase-shifted signals for each input. Temperature readings (T) are linearized with a third-order polynomial and a single offset is used for calibration. Calibration data is typical for each sensor, and must be stored in memory to be retrieved at the time actual measurements are taken.

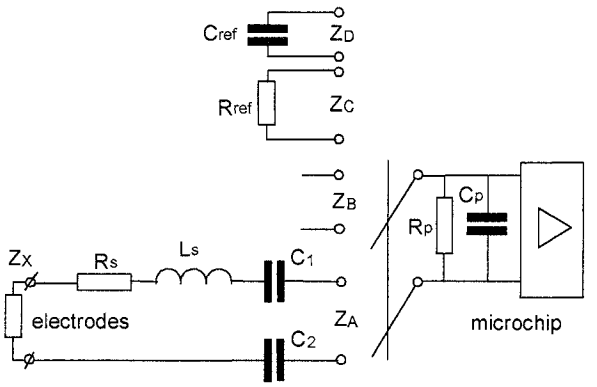

Fig. 13.5. Simplified electric model for the sensor measuring rods and chip input circuitry. Z_B is left open, and the DC-blocking capacitors C_1 and C_2 are considered to be much larger than the capacitive components in Z_x

Serial data coming out of the chip must be processed before the dielectric properties of the material under test become available. A multi-purpose microprocessor, a hand-held computer or a PC can do this job. From the serial data and previously stored calibration data for R_{ref}, C_{ref}, C_p, R_p, L_s, and R_s, and based upon complex arithmetic, the impedances Z_A to Z_D are computed first. Next the unknown impedance Z_x can be obtained. Finally, from this impedance, the dielectric properties ε and σ are computed [8, 22].

For a prototype sensor the ε- and σ-scales and the electrical path length compensation parameters were obtained by placing the electrodes in reference media. Air, tap water ($\sigma \approx 0.002$ S/m), and water of two other conductivities (0.1 S/m and 0.2 S/m) were used. The ε-scale was calibrated between $\varepsilon = 1$ for air and $\varepsilon = 80.3$ for tap water at 20°C. The σ-scale was determined for $\sigma = 0$ in air and $\sigma = 0.2$ S/m in water. L_s was found from the measurements in water at $\sigma \approx 0.002$ S/m and $\sigma = 0.2$ S/m. Water with $\sigma = 0.1$ S/m was used to adjust R_s such that ε-readings at all three conductivities were equal. The calibration software used a recursive approach to yield the dielectric calibration data. Tests with the sensor showed that ε could be measured with an accuracy of ±1 on a scale of 1–100 and a resolution of 0.1 in a temperature range from 15 to 25°C. Based on the temperature sensor SMT160-30 (Smartec, Breda, the Netherlands), readings have an accuracy of 0.5°C with a resolution of 0.1°C, in the operating range from –5 to 50°C.

13.2.3 Temperature Corrections

FD sensor readings are dependent on temperature. In the soil top layer, where temperature is very much dependent on sunlight, sometimes large temperature fluctuations are seen during the day. To allow for on-line correction, temperature is measured in the sensor. Little is found in the literature about the influence of soil texture and density on the temperature behavior of soil water content and EC. Recently it has been shown that the temperature behavior is dependent on soil texture [23]. Positive as well as negative effects have been seen for different soil types. This makes temperature corrections rather ambiguous. Nevertheless, for permittivity and conductivity separately we can perform some general corrections. The permittivity of pure water at a specific temperature can be obtained from [24]:

$$\log \varepsilon_{\text{water}}(T) = 1.94404 - 0.001991\ T. \tag{13.1}$$

This function was specified over a temperature range from 0 to 40°C with a maximum error of 0.3%. A simpler equation can be used, such as the following approximation of Eq. (13.1):

$$\varepsilon_{\text{water}}(T) = 80.327 - 0.368(T - 20). \tag{13.2}$$

EC depends on T and the dissolved ion types, which makes it impractical to handle this parameter just as it is measured. Growers use EC referred to a predefined reference temperature (T_{ref}), for instance 20°C or 25°C. For each water–salt mixture a specific temperature coefficient (α_i) should be used. This referenced conductivity ($\sigma_{T\text{ref}}$) can be computed from [25]:

$$\sigma_{T\text{ref}} = \sigma[1 - \alpha_i (T - T_{\text{ref}})]. \tag{13.3}$$

For average soil types a value of $\alpha_i = 0.0216°C^{-1}$ [26], and for water with dissolved NaCl, $\alpha_i = 0.0225°C^{-1}$ may be used.

13.3 FD Sensor for Water Content and Bulk EC in Soil

Based on the microchip described in the previous section, a water content FD sensor (see Fig. 13.6) was developed [18]. This sensor determines the complex permittivity of soil from the electric impedance at a single frequency (20 MHz). The complex permittivity can be related to bulk electrical conductivity (σ) and volumetric water content (θ) after calibration for a certain soil type [6, 18, 27]. By using the microchip, the sensor is solid state, robust, and needs no maintenance and no repeated calibrations. It has three in-line electrodes of which the outer two are electrically connected together and behave as a guard similar to the working of a coaxial probe. It has been shown that it can operate on a long-term basis and can be produced in large quantities at a low price [20, 28]. Currently it is available as the WET-sensor (Delta-T Devices Ltd, Cambridge, UK).

The validation of the FD sensor for permittivity was done by placing a number of FD sensors in reference liquids: pure water, a 1:2 water–ethanol mixture, and

water-saturated glass beads (0.2 mm) at a constant temperature of 20°C. Conductivity was varied using increasing amounts of NaCl. It was shown that after calibration the sensors operated well and that the accuracy for permittivity was ± 1% over the full-scale range from 1 to 80. The sensors were also validated for conductivity. The accuracy found for conductivity was ± 1% for a full-scale range from 0 to 0.2 S/m. These observations were based on a limited number of sensors and were done for a full-scale calibration of 0.2 S/m [8].

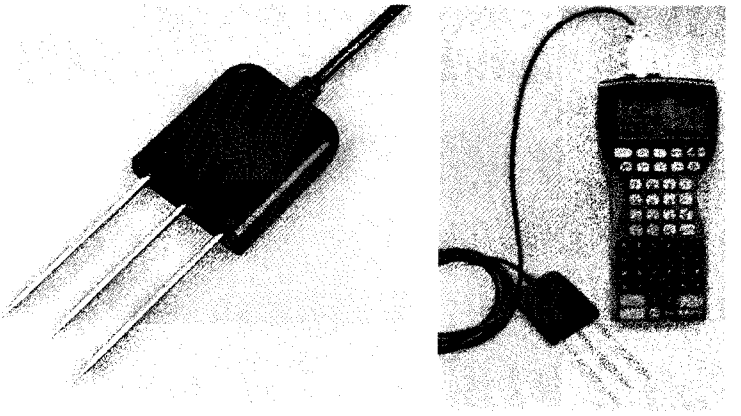

Fig. 13.6. FD sensor for soil water content, EC, and temperature (*left*). The dimensions of the housing are 46×55×12 mm^3, and the electrodes have a length of 68 mm, each spaced 15 mm from each other. FD sensor connected to a PSION Workabout hand-held computer (*right*)

The sensors were used in several applications, and also calibrated for higher EC ranges up to 0.5 S/m. As will be shown in a later section, the sensors can be used to measure pore water conductivity as well. For that, σ is multiplied by a factor larger than one, which is proportional to the reciprocal value of the water content. Hence, errors in σ will be multiplied by this factor as well, so the accuracy of σ plays an important role. The factor becomes larger at lower θ levels, and the relative accuracy for σ gets lower, at lower σ-values, as is the case for dry agricultural soils ($\sigma < 0.1$ S/m, $\theta < 15\%$). For this reason extra attention was paid to the σ-linearity of the sensor, especially in the lower range ($\sigma < 0.1$ S/m).

The σ-linearity of the FD sensor was evaluated by measuring σ for eight different sensors in a number of water–salt mixtures. To see whether the calibration range influences the linearity of σ, this was done for three calibration ranges from 0 to σ_{max} (0.2, 0.4, and 0.8 S/m). First, the sensors were calibrated by using the procedure described in the previous section at three values for σ (0, ½σ_{max}, and σ_{max}). Then, water–salt mixtures were made in the range from 0.01 to 0.5 S/m by mixing NaCl with water at a temperature of 20°C starting at the lower σ and

adding salt to the mixture for each new experiment. Conductivity of the reference mixtures was measured using a four-point electrode LF conductivity meter from Profilab (WTW-LF597-S) working at 1 kHz with a standard conductivity cell, Tetracon 325 (Wissenschaftlich Technische Werkstätten GmbH, Germany).

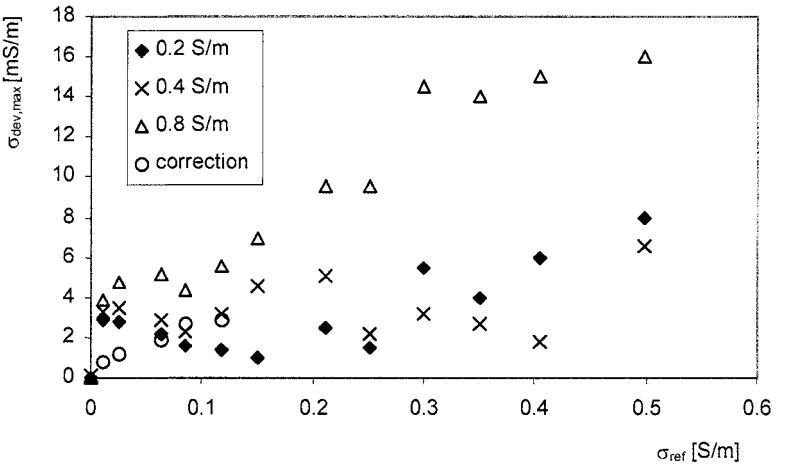

Fig. 13.7. Absolute maximum measured deviation in conductivity for eight FD sensors ($\sigma_{dev,\,max}$) versus reference conductivity (σ_{ref}) at three full-scale calibrations (σ_{max} = 0.2, 0.4, and 0.8 S/m)

Figure 13.7 shows the results of these experiments, where σ_{ref} indicates the conductivity measured with the LF meter in the reference mixtures, and $\sigma_{dev,max}$ is the maximum deviation for all 8 eight FD sensors found between σ_{ref} and the measured value (σ). We can see a sinusoidal behavior of the error that is dependent on the full-scale calibration range. This is due to the fact that a simplified model is used to compensate for the electrical path length of the electrodes. For the two calibration ranges 0.2 S/m and 0.4 S/m we see further that the errors become close to zero near the maximum conductivities at which the sensors were calibrated (σ_{max} = 0.2 and 0.4 S/m). Furthermore we see that the errors become larger outside the calibration range. Here obviously the model for electrical path length compensation does not work that well. Table 13.2 gives an overview of the maximum deviation found for all calibration ranges including the accompanying full-scale error. We see that the error is slightly more than the ± 1% found before [8]. Therefore, the sensors should be calibrated in the range where the expected measured values for σ will be.

Table 13.2. Maximum found deviation in conductivity for all 8 FD sensors within the calibration range, including the belonging full-scale error

Range (S/m)	$\sigma_{dev,max}$ (mS/m)	Error (% f.s)
0.2	3	1.50
0.4	5	1.25
0.8	16	2.00

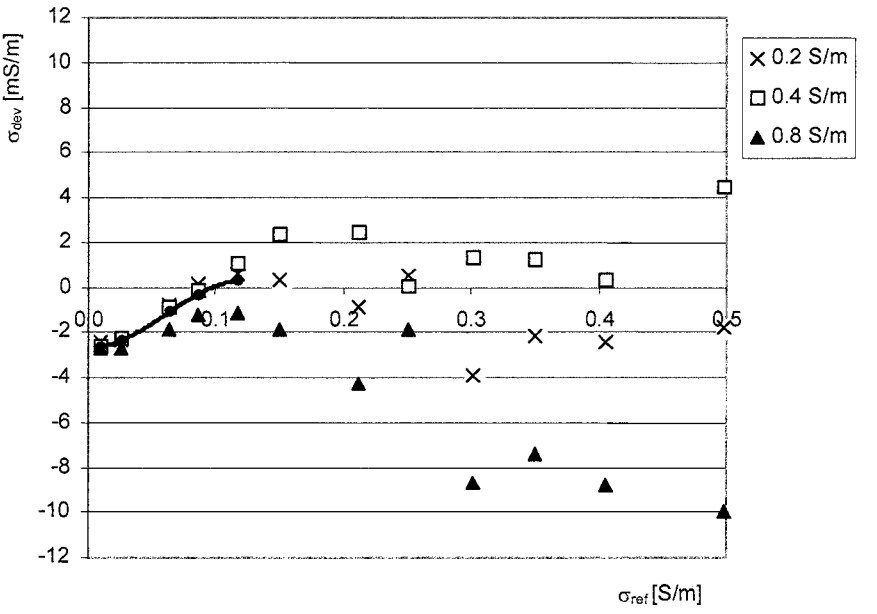

Fig. 13.8. Mean value of the measured deviation in conductivity for all FD sensors plotted against the reference conductivity.

Since the errors seem to correlate with conductivity due to the mismatch of the electrical path length compensation, we looked for ways to compensate for this systematic error. In Fig. 13.8 the mean value of the deviation for all 8 FD sensors for each used reference value is plotted against the reference values. We see clearly the sinusoidal behavior of the error, though it is different for each calibration range. For the two ranges 0.2 and 0.4 S/m the mean error stays within about 1.5% of the absolute value apart from conductivity values below 0.1 S/m. The errors are larger for the 0.8 S/m range. But, this range is rarely used in agricultural applications. At low conductivities ($\sigma < 0.1$ S/m) we see a significant and typical a-linear behavior, which seems to be independent of the full-scale calibration. Here, especially for $\sigma < 0.05$ S/m, the FD sensor systematically overestimates the conductivity by about 1–2 mS/m. Since this range is rather important for soils

used in agricultural a correction is proposed for $\sigma < 0.05$ S/m, which leaves values above 0.05 S/m untouched. This correction can be used, irrespective the calibration scale. Figure 13.8 also shows a polynomial fit of the third order, common for the two calibrations for 0.2 and 0.4 S/m over the range from 0 to 0.1 S/m. Based on this fit the following equation was obtained for the corrected conductivity (σ^*):

$$\sigma^* = \sigma + a_0 + a_1\sigma + a_2\sigma^2 + a_3\sigma^3, \tag{13.4}$$

where we have assumed that $\sigma_{dev} \ll \sigma$, so we can replace σ_{ref} with σ as measured. For this polynomial fit the following coefficients were found: a_0=-2.6506×10^{-3}, a_1=-3.1322×10^{-3}, a_2=0.64974, and a_3=-3.4724 (R^2=0.999). The results of this correction are showed in Fig. 13.7. We see that the errors for $\sigma < 0.05$ S/m are lower after correction. We can conclude that the full-scale accuracy for σ is 1.5%. After correction, at small values for $\sigma < 0.05$ S/m, for the two ranges of 0.2 and 0.4 S/m, an absolute accuracy better than ± 3% can be obtained.

The relationships between ε, σ, and θ, strongly depend on soil density (ρ) and texture [6, 29]. Therefore, to obtain accurate readings, a soil-specific calibration is needed. This calibration is obtained by weighing soil samples during drying, while taking readings with the sensor. This gravimetric method gives reliable data under well-controlled conditions. For θ often the calibration Topp–curve is used [6]. This curve was obtained for sand and a number of sandy loam and clay–loam soils, by using the TDR principle at 150 MHz. It is used for an "average soil" and can be approximated with a third-order polynomial. Sometimes it is used in a simpler form:

$$\theta = 0.115\sqrt{\varepsilon} - 0.176\,. \tag{13.5}$$

For soils commonly used in horticulture, the accuracy found with this curve is ± 5%. To test the working of the soil-water-content FD sensor based on Eq. (13.5), an experiment was conducted with soil sampled from the top layer of a yellowish brown forest soil containing 18% clay and 3% organic matter [30]. The samples were air dried to reach weight equilibrium. Then θ was measured after drying in an oven at 105°C for 48 hours. A plastic container was filled with the dry soil and weighed to calculate its soil mass and volume. Then the amount of water to get a specific θ was calculated. Next, the dry soil was mixed with the water and poured into the plastic container. Then the soil volume in the container was recalculated and the final θ was determined. These samples were stored for 2 days to let the water redistribute and the temperature reach equilibrium. Thereafter the samples were measured with an FD sensor on three consecutive days, and average values were used to obtain the calibration curve, which were compared to Topp data (θ_{Topp}). The results for soil moisture from the experiment are given in Table 13.3. For this specific forest soil, the Topp curve slightly underestimates the actual moisture content (see Fig. 13.9). In the range from 0 to 35%, an accuracy of ±1.1% was achieved, which is nearly as low as the accuracy for ε.

Table 13.3. Results of ε measured with the FD sensor (ε_{FD}), volumetric water content as calculated with the oven dry method (θ), volumetric water content according to Topp (θ_{Topp}), and difference between θ and θ_{Topp} ($\Delta\theta$)

ε_{FD}	θ (%)	θ_{Topp} (%)	$\Delta\theta$ (%)
2.54	0.00	0.73	0.73
3.58	4.51	4.16	–0.35
5.50	10.35	9.37	–0.98
7.76	15.18	14.44	–0.74
12.85	24.74	23.62	–1.12
16.40	29.51	28.97	–0.54
18.79	32.64	32.25	–0.39
20.14	34.19	34.01	–0.18

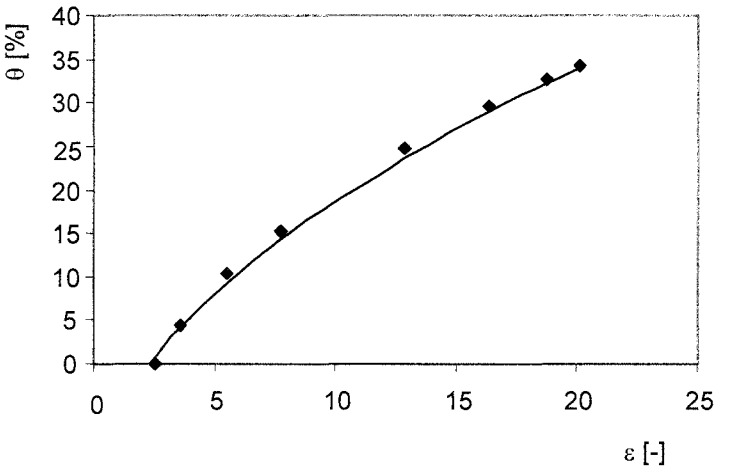

Fig. 13.9. Permittivity (ε) and soil water content (θ) measured for a forest soil (♦), related to the Topp-curve (—)

13.4 A Pore Water Conductivity Sensor for Growing Substrates

Traditionally TDR and FD methods measure permittivity (ε) and bulk conductivity (σ). Growers often refer to σ by using the term EC for electrical conductivity. EC here reflects the total electrical conductivity of the entire matrix containing substrate material, water, nutrients and air, which is strongly dependent on water content (θ) and subsequently ε. Since plants take up only water-dissolved fractions, growers are mostly interested in the EC of the water that can be extracted from the substrate matrix, for instance with a syringe. This so-called pore water conductivity (σ_p) relates to σ, but is dependent on ε. Straightforward measurement of σ with the FD sensor is therefore not useful for growers using substrates as for instance mineral wool mats or *Rockwool* (Grodan, Roermond, the Netherlands). Soil-based growers normally obtain σ_p by taking a soil sample. This sample is then mixed with a known volume of water to let the nutrients dissolve. Next they measure the EC in the aqueous solution with a standard EC meter. In case the amount of added water has the same volume as the soil sample, this method is referred to as "the 1:2 extract method." The pore water EC value is found by multiplying the measured value by a factor of two [31].

The FD sensor, based on the microchip, is capable of measuring σ, as well as ε and temperature (T). Therefore, by measuring σ and correcting for ε and T, one can obtain σ_p with this sensor. This involves only a simple and straightforward model. This model was used to measure σ_p in situ in soil, for precision agricultural applications [32], and it describes the relationship between σ_p and the bulk soil values for ε and σ as measured with the FD sensor:

$$\sigma_p = \frac{\varepsilon_{water}\sigma}{\varepsilon - \varepsilon_{\sigma=0}}. \tag{13.6}$$

In this equation ε_{water} is the pure water permittivity corrected for temperature (see Eq. 13.2), and $\varepsilon_{\sigma=0}$ is an offset value. This offset can be obtained from ε and σ measured at two arbitrary free water content values and is not the value for ε when $\theta = 0$, but specifically for $\sigma = 0$. For a number of soils, empirically, values between 1.9 and 5.8 were found for $\varepsilon_{\sigma=0}$. These values are dependent on soil type, density, and the pin-type configuration [33]. For Eq. (13.6), it was assumed that the water is not bound to the soil matrix. Therefore, the model can not be used for bound water. Neither can it be used for conductivity due to ions moving through the lattice of ionic crystals in a dry or almost dry soil. For sand, the free water content corresponds to $\theta > 0.01$. For clay this is $\theta > 0.12$ [34]. As a rule of thumb the model applies for most normal soils if $\theta > 0.10$. Since it uses ε rather than θ, no calibration for θ is needed, and sensor working is not influenced by the soil–electrode contact and soil texture.

Since contact problems have only a minor effect on the measurements, a new sensor with a single and small sensor tip was developed (see Fig. 13.10, left). This sensor allowed for easy insertion into soils, but it was meant for measuring σ_p

only. It uses the same electronics as the FD sensor described in the previous section, but with a slightly higher measuring frequency of 30 MHz. The electronics are placed in a cylinder of a hard polyurethane molding at the top of the sensor rod. This rod is 10 cm long and has a diameter of 5 mm. It ends in a sharp point to facilitate insertion of the electrodes. The sensor tip is about 15 mm long and split into two metal electrodes separated from each other by a thin sheet of isolating material. The latter is a fringing field configuration where field lines concentrate just around the sensor tip. A temperature sensor is located close to the sensor tip to facilitate temperature measurements. A flexible polyurethane output cable contains the RS232 signal and power supply wires. This cable connects the sensor to a hand-held computer that runs signal-processing software.

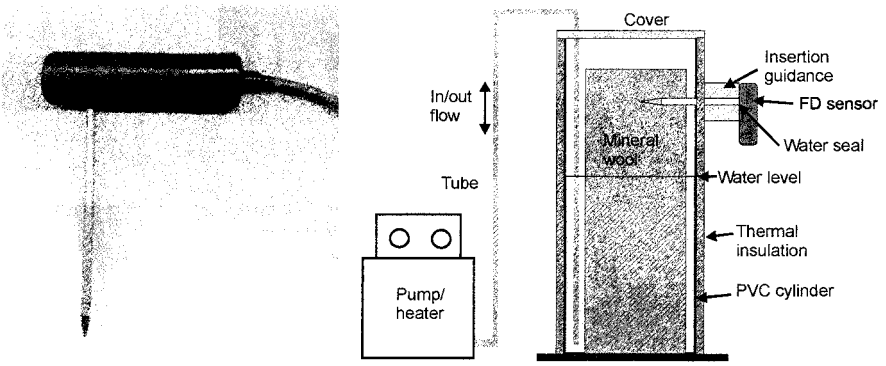

Fig. 13.10. Sensor for measurement of σ_p in soil (*left*). Experimental set-up (*right*)

It was shown that this sensor could be used for growing substrates as well, and for *Rockwool* a value for the offset $\varepsilon_{\sigma=0}$ of 4.1 was found [33]. For growers, this provides a new and more manageable way to measure in situ pore water EC, especially for hand-held application. In greenhouses, however, the encountered pore water EC levels in growing substrates are much higher than those found in soils. Furthermore the daily fluctuations of temperature are large. Therefore, the calibration of the model, the operating range, and the effect of temperature for application in mineral wool growing substrates were points of further study.

The performance of the sensor was studied in a *Rockwool* growing substrate at different values of EC, water content, and temperature, while it was connected to a PC [35]. The set-up (see Fig. 13.10, right) consisted of a vertical-placed PVC cylinder with an inner diameter of 15 cm and an height of 88 cm. The whole cylinder was thermally insulated. The top was covered to prevent evaporation and temperature gradients, and the bottom was sealed so as not to leak any water. Inside the cylinder a slab of growing substrate material was placed, filling about 80% of the inside of the cylinder. The sensor was inserted into this slab, horizontally through the wall of cylinder, about 10 cm under the top of the slab. An insertion guidance

block was used to support the sensor to prevent it from leaning downwards. The sensor shaft was sealed with a silicone kit to make it watertight. Once inserted into the growing substrate the sensor was kept in place to keep the contact between the electrodes and the growing substrate intact.

The growing substrate around the sensor tip had to be brought at several levels of θ, σ_p, and T. Drying the sample through evaporation was not possible since the salt concentration in the pore water would then rise. Only a method that saturates and de-saturates the growing substrate sample in equal portions could be used. Therefore, water–salt mixtures were pumped in and out the container via a flexible tube fitted to a thermostatic bath containing a pump/heater combination (Ultra-Thermostat, COLORA, Germany) at a very slow rate.

Prior to the experiment the sensor was calibrated for ε and σ by measuring with reference values for air ($\varepsilon = 1$, $\sigma = 0$) and tap water ($\varepsilon = 80.3$, $\sigma \approx 2$ mS/m), and with water of two known conductivities (0.1 and 0.2 S/m) at 20°C. The temperature was calibrated using a single-point offset. Then, reference water–salt solutions were made by mixing NaCl with water at a reference temperature of 20°C. A Profilab WTW-LF597-S conductivity meter working at 1 kHz with a Tetracon 325 conductivity cell (Wissenschaftlich Technische Werkstätten GmbH, Germany) was used for this. Four EC values (σ_{ref} = 0.02, 0.05, 0.11, and 0.31 S/m) were taken by starting at the lower EC level and adding salts to the solution for each new experiment. Since salt and water have a different mobility, and to be certain of having the correct σ_p inside the growing substrate, the sample was slowly saturated and de-saturated several times to allow salt to fully penetrate the material. At the beginning of the measurement, the sample was completely immersed in water. Next, slowly and stepwise, it was de-saturated by pumping the water out of the cylinder. This was done until the sensor indicated a very low ε- or σ-value. The pump was stopped at water levels of +5 (saturated), –7, –10, –12, –15 and –18 cm, all referenced against the top of the substrate slab. During each stop, readings for ε, σ, and T were taken. Thereafter the cylinder was brought back to full saturation, and possible hysteresis effects were checked. A complete cycle took about 4 hours. Although exact values for θ could not be obtained, a broad range of θ-values was available. This procedure was repeated four times, by setting the thermostat subsequently at 10, 20, 30, and 40°C. Temperature and water content changes were applied four times at each EC value.

The experiment yielded 96 readings in total, for six water levels, four EC levels, and four temperatures. Since ε follows the wet–dry–wet cycles for θ, it behaves in a sawtooth manner. Readings for ε drop down to about 15 at low θ, and go up to about 70 at saturation (see Fig. 13.11, top). The temperature was set at a fixed level for each wet–dry–wet cycle (see Fig. 13.11, bottom). Based on Eq. (13.6) and the readings for σ, ε, and T, values for σ_p were computed. Figure 13.12 shows the conductivity for the original mixture (σ_{ref}), σ as measured directly with the sensor, and σ_p as computed, based upon $\varepsilon_{\sigma=0} = 4.1$, and referenced to 20°C with $\alpha_i = 0.0225°C^{-1}$ for NaCl (see Eq. (13.3)). For a good working sensor, the curves for σ_p and σ_{ref} should be identical.

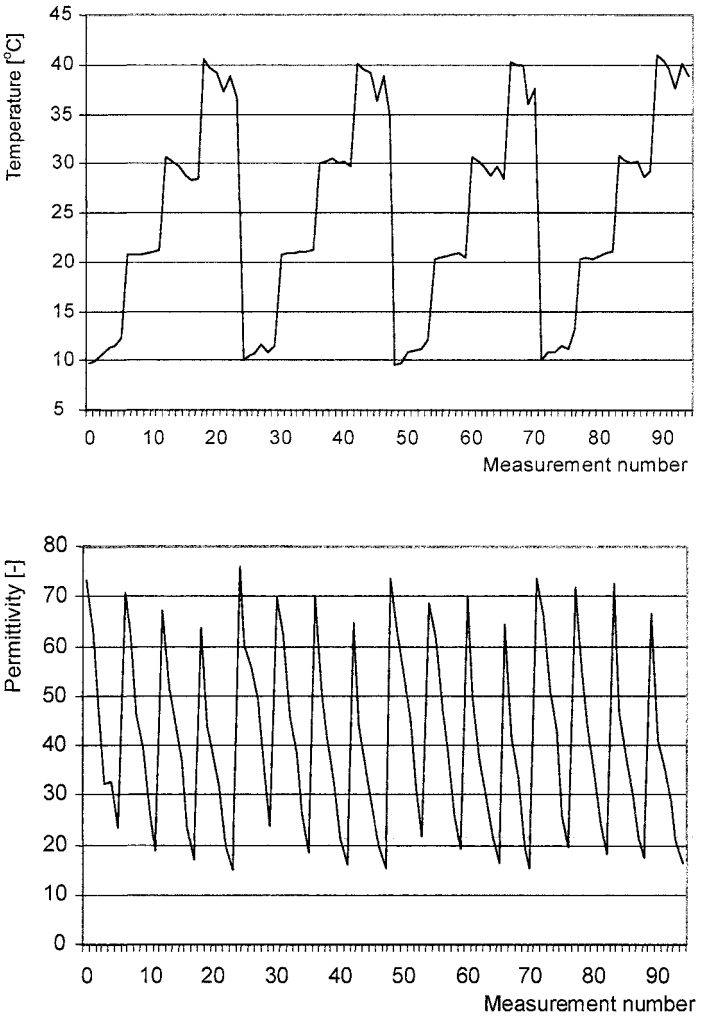

Fig. 13.11. Permittivity (*top*) and temperature readings (*bottom*) with measurement numbers on the x-axis

In spite of the temperature corrections for ε_{water} and σ, it can be seen that there is still a dependency on temperature (see Fig. 13.12). At higher temperatures, σ_p tends to decrease, while at lower temperatures there is a little overestimation of σ_p. A second-order fit could correct for this, but its effect was not fully analyzed. The performance of the temperature correction is considerably influenced by α_i. Although we used a fixed value for α_i of 0.0225°C^{-1} for NaCl, a better a correlation for σ_{ref} and σ could be obtained by using a coefficient of about 0.01°C^{-1}. It seems that the impact of the medium, with respect to the salt-type mixture used, has a

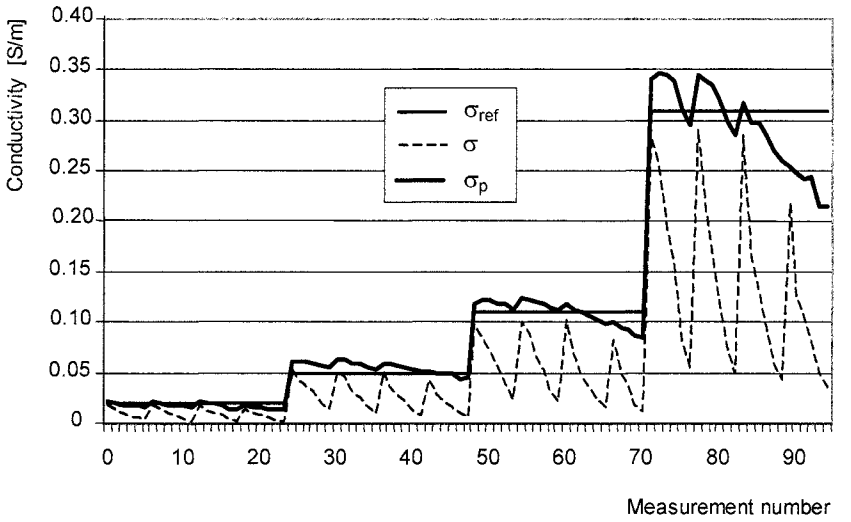

Fig. 13.12. Conductivity readings (σ), reference values (σ_{ref}), and computed pore water conductivity (σ_p) at each measurement

more complex nature than expected. Since we might expect that the medium used has no effect upon ε itself, probably pore binding effects influence $\varepsilon_{\sigma=0}$. There is a dependency on θ which leads to lower σ_p at lower θ. At high values of σ and at higher T, the absolute errors become larger. Further analyses should show whether the algorithm needs adaptation. This could be done by tuning $\varepsilon_{\sigma=0}$. At higher θ (> 20%) the sensor performs well. For practical applications this is good, since growers keep their substrates normally at water content levels between 40 and 70%. The model works reasonably well over the range from 0.02 to 0.2 S/m; but nevertheless, the mean error is 2.1%, with a standard deviation of 14.8%. The experiment was performed with a *Rockwool* substrate, which might behave differently compared to other substrate media. Furthermore only a single salt (NaCl) was used. Different salts or salt mixtures might have other effects upon the behavior of the sensors. Further research should focus on different salt-type mixtures.

From the experiment we may conclude that the sensor has a reasonable performance over the range studied (σ_p = 0.02–0.31 S/m), but not at low water contents (θ < 20%). There is a dependency on θ and T. At high temperatures (T > 30°C) and at high EC values (σ_p > 0.2 S/m) absolute errors become large, even up to 0.09 S/m. The overall standard deviation error is 14.8%. Further research to enhance the model is likely to succeed and therefore certainly worthwhile to perform.

13.5 Monitoring the Strength of Young Concrete

Information about the development of the strength of young concrete during the first 28 days after pouring is the basis for deciding on formwork removal or the application of pre-stresses in construction engineering. Measuring the strength of young concrete may lead to faster formwork removal and fewer risks, and therefore has economical benefits [36]. Hydration of concrete causes a decrease of free water, an increase of compressive strength, and a temporal temperature rise in the mixture. To monitor hydration and strength development, currently the maturity method is applied. It uses in situ temperature monitoring in parallel with maturity and laboratory stress tests at the concrete manufacturer. In the Netherlands this method is standardized [37] and it works similar to, though in principle it is different from, the American standard procedure [38]. Both methods are commonly accepted, but time consuming and therefore costly when used under practical circumstances. The use of dielectric spectroscopy might be a good alternative for making in situ sensors.

During the hydration of concrete, the cement reacts with the water. This causes the concrete microstructure to grow and this in turn means that the concrete compressive strength increases. At the same time the amount of free water in the mixture decreases. In fact, more structure means less water and more strength. The decreasing amount of water and the increasing amount of structure influence the dielectric properties of the concrete. The conductivity (σ) and permittivity (ε) of the mixture therefore reflect the increasing strength of the concrete and can be obtained after a concrete mixture-specific calibration. Many authors have described the dielectric behavior of concrete [39– 41]. Later it was shown that the FD sensor described previously offers a reliable non-destructive way to determine strength in situ, independent of the weather and other environmental conditions [42, 43]. This method was patented [44]. Based upon this principle, a sensor for monitoring the strength of young concrete was developed [12, 36] and made available commercially (ConSensor b.v., Rotterdam, the Netherlands).

The sensor consists of two stainless steel electrodes mounted in a watertight housing which includes the dielectric chip for measuring conductivity and temperature. A temperature sensor is placed in one of the rods. It connects via an RS232 connection to a hand-held computer (see Fig. 13.13). The sensor itself can be inserted into an electrode set that can be positioned in a predrilled hole in the concrete formwork by using an insertion tool. This insertion tool is in fact a sensor dummy that can temporarily be fixed to the formwork. Once the electrode set is cast in, it remains in the concrete permanently. The FD sensor can be used to monitor strength at multiple locations, just by plugging it into the electrode sets. A hand-held computer (PSION Workabout, Psion Teklogix Gmbh, Willich, Germany) computes the concrete strength parameters based upon the measured conductivity. PC software is used for further analyzing the collected data and for making calibration curves for the different concrete mixtures.

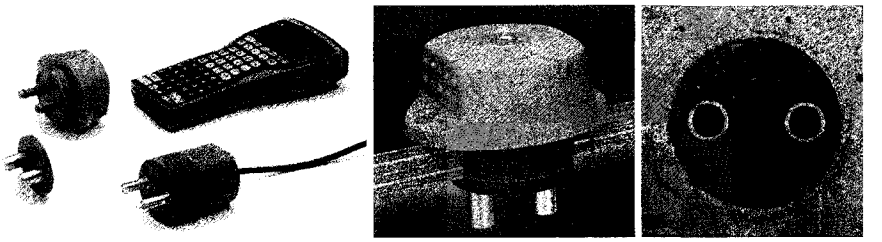

Fig. 13.13. The ConSensor system containing a PSION Workabout, sensor with cabling, electrode set, and an insertion tool with plastic cap (*left*); electrode set and insertion tool with plastic cap, inserted into a predrilled hole in formwork before molding (*middle*); electrode set enclosed in concrete after molding (*right*)

To evaluate the suitability of this FD sensor, its working was compared with the standard maturity method under practical circumstances. During the reconstruction of the Suurhof bridge in the Europoort region in the Netherlands, the concrete strength development in the new pillars of its foundations was monitored using both methods. In these foundations an exceptionally high amount of rebar steel was applied, which was a good opportunity to verify also the influence of rebar upon the dielectric measurements.

Before the in situ tests, a calibration for the specific concrete mixture was performed. Several small cubes of the mixture were made for this. One cube was used to measure dielectric data during the hydration process, which data were stored on a PC. Another cube was tested with the traditional maturity method by taking temperature readings. As reference for these measurements, tests were performed in the laboratory by pressing the cubes at regular time intervals and obtaining the compressive strength (*CS*) at the moment of collapse. The data was entered into a program, which calculated a calibration curve linking the dielectric data to the actual strength of that mixture of concrete. At the construction site this calibration curve was used to compute concrete strength with the hand-held terminal. At the site there were ten pillars. Two FD sensors were placed in every pillar. Two temperature sensors for the maturity method were placed nearby, one in the center of a pillar and one close to the outer site of the pillar. The measurement results, taken at two phases (Phase I and Phase II) of the project, four months apart in time, are given in Table 13.4.

Based upon this data a calibration curve (see Fig. 13.14) was obtained for the FD sensor (CS_{FD}) as well as the maturity method (CS_M):

$$CS_{FD} = 1.9184\sigma^{-0.8005} \quad (R^2 = 0.987) \tag{13.7}$$

$$CS_M = 13.415 \ln(M) - 74.253 \quad (R^2 = 0.952). \tag{13.8}$$

Table 13.4. Calibration results with compressive strength (*CS*), conductivity (σ), and maturity (*M*) in arbitrary units

CS (N/mm^2)	σ (S/m)	M (—)
16.4	0.070	832
19.9	0.052	1,400
24.5	0.040	1,469
28.4	0.035	2,064
30.5	0.030	2,681
34.6	0.027	3,836
44.3	0.021	7,510
47.6	0.020	4,925
50.5	0.015	12,400
56.2	0.015	17,480

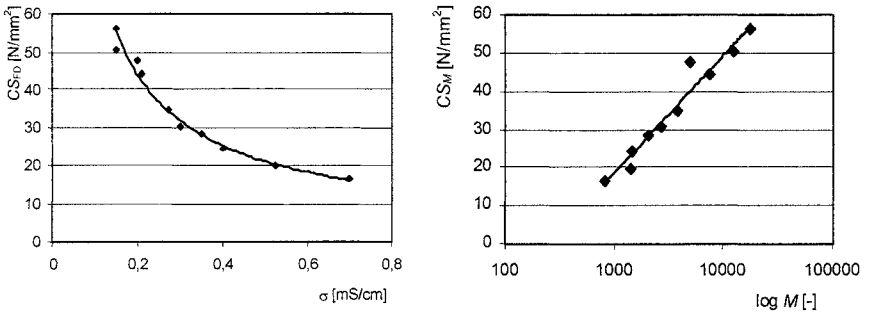

Fig. 13.14. Calibration curves for FD method (*left*), and maturity method (*right*)

Based on the calibration curves and by using the measured data (Table 13.4), for both methods strengths were recalculated and then plotted (see left part of Fig. 13.15). We can see that the two methods correlate rather well ($R^2 = 0.968$). Based upon the accuracy specifications for σ (see Fig. 13.8) for the FD method (resolution = 1 μS/m and 5% for $\sigma < 0.1$ mS/m), the confidence intervals were plotted as well. We can see that for higher strengths and at lower conductivities the accuracy is reduced. This is due to the power law curve that becomes rather steep in this range (see Fig. 13.14, left). Although the readings still fall within the confidence interval, the absolute deviation between CS_M and CS_{FD} is ±10%. The linearity stays within 0.05% over the measuring range. Next in situ measurements, first in Phase I and then in Phase II, were taken (see Fig. 13.15, right).

Looking at the in situ compressive strength data for phase I (see Fig 13.15, right), it can be noted CS_{FD} and CS_M differ substantially, up to 11 N/mm^2. It appears that the maturity method yields slightly higher strengths. Since the pillars contained a lot of rebar steel, it was suspected that the dielectric measurements

were influenced by the rebar (see Fig. 13.16, left). After ruling out some possible sources of error such as initial water conductivity and variability due to sensor placement, new measurements were taken (Phase II), taking special care with the location of the FD sensor relative to the rebar (see Fig. 13.16, right). The length of the electrodes is 40 mm. The distances between the tip of the sensor electrodes and the rebar steel were classified as "large," "small," and "very small" respectively for distances of more than 50 mm, between 10 and 50 mm, and less than 10 mm (see Table 13.5). The distances sometimes became very small, even a few millimeters. In some cases the electrodes were even electrically shorted. The results of these measurements are plotted in Fig. 13.15 (right). For the three classes the mean values for the difference between CS_{FD} and CS_M were calculated (see Table 13.5).

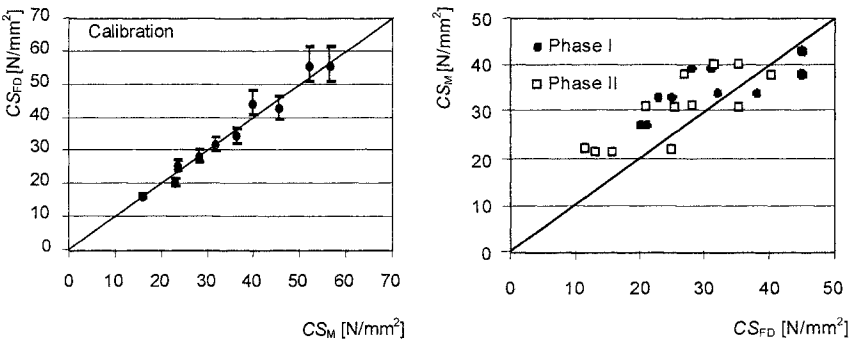

Fig. 13.15. Calibration for compressive strength (•), maturity method versus the FD method, including confidence intervals (—) for the FD sensor (*left*). Compressive strength measured in situ with both methods (*right*). The 1:1-line is shown in both graphs

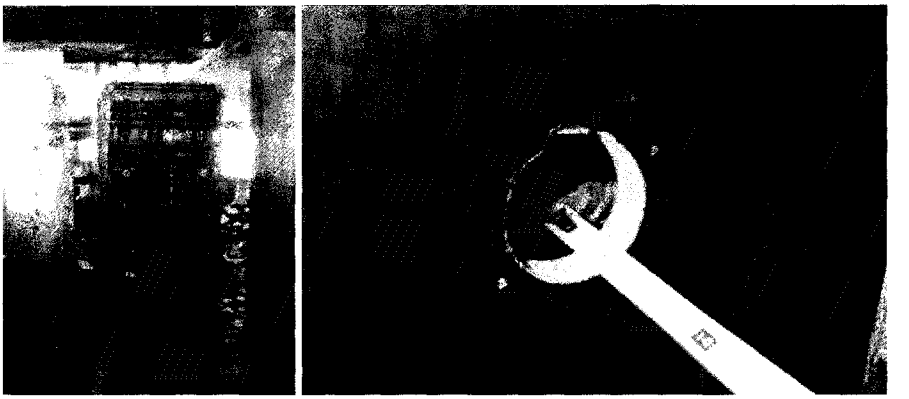

Fig. 13.16. Pillars contain a lot of reinforcement steel (*left*). At one measuring point even the sensor electrodes were in contact with the reinforcement steel (*right*)

Table 13.5. Strength differences in relation to sensor–steel rebar distances

Distance of sensor electrodes to steel rebar (mm)		Mean ($CS_M - CS_{FM}$) (N/mm^2)
> 50	(large)	–3
10–50	(small)	4
0–10	(very small)	9

Though the number of measurements is too small to draw any statistically significant conclusions, we can see that in those situations where the electrodes are close to the rebar ("very small"), there is a large difference in strength. When the electrodes have a distance larger than 1 cm, the errors are smaller and in the order of the measuring noise. It seems that the highly conductive steel leads to a higher conductivity and consequently a lower compressive strength when using the FD method.

We may conclude that for monitoring the strength development of young concrete, the FD sensor can be used as a practical alternative to the maturity method. The calibration was shown to be robust and comparable to the standard maturity method. No permanent measurement is needed; with portable equipment as many measuring points as required with one sensor can be taken. However it was seen that the near contact of the FD sensor electrodes with the rebar steel results in a higher value of the measured conductivity, and consequently an underestimation of strength. A practical solution for this is to keep a safe distance of at least 50 mm between the electrodes and the steel rebar.

13.6 A Dielectric Tensiometer to Measure Soil Matric Potential

Water content sensors, as described in the previous sections, measure the amount of water in the soil matrix and can indicate the amount of water that should be given to plants. On the other hand, tensiometers measure soil matric potential and indicate the moment at which plants should be given water. There is a relation between these two, which is described by the pf-curve [45]. For good water management both parameters are needed. If the pf-curve is known, only one parameter is needed. The pf-curve has an exponential behavior and depends on soil texture and density. Since both of these soil features vary greatly under practical circumstances, and soil behaves differently for wetting and drying, there is still a need for both types of water sensors. An FD sensor for soil water content was described in an earlier section; here we will discuss the use of the FD method to build a soil matric potential sensor.

For irrigation purposes normally water-filled hydraulic tensiometers are used [46, 47]. They consist of a ceramic cup placed in the soil, connected to a water tube with a mechanical or an electronic pressure gauge on top. These sensors are not so suited for automatic irrigation systems, since they need regular calibration and maintenance, such as refilling with water, and their working range is restricted

for dry soils to about –85 kPa. In spite of the drawbacks, lacking a better alternative, and due to the need to save water, in semi-arid areas as well as in greenhouses hydraulic tensiometers are still being used. An alternative design, nowadays known as resistance blocks has been proposed [48]. Here, the AC resistance between two electrodes molded into a porous material is measured and calibrated against matric potential. Later, a conductivity sensor was used to measure water content inside a water permeable container filled with quartz sand [49]. These granular-type sensors came onto the market as the WATERMARK sensors (Irrometer, Riverside, CA, USA) and were optimized for use between –10 and –100 kPa. Though cheap, they were inaccurate and their calibration varied for different soils [50].

Hilhorst and de Jong [51] reported for the first time the use of a dielectric sensor to build a solid state tensiometer. This dielectric tensiometer measures matric potential indirectly by measuring the water content inside a ceramic material which is in equilibrium with the soil water. Once the sensor is inserted into soil, the water potential inside the ceramic will become equal to the soil water potential. Because the water retention characteristic (pf-curve) of the ceramic is known, matric potential can be calculated from the water content readings. These authors showed the results of a prototype based on the use of glass beads as the porous material. A decade later, the first version of this sensor was launched as the Equi-Tensiometer (UP Umweltanalytische Produkte GmbH, Cottbus, Germany), which was based upon the MR2 Theta Probe (Delta-T Devices Ltd, Cambridge, UK) working at 100 MHz. This sensor was also of the granular matrix type. This influences its accuracy, and its large size made its response slow. Recently, a newer version of the Equi-tensiometer was launched, which is based upon a new, more stable, and smaller substrate material [52]. It has a working range from 0 up to –1500 kPa. Or and Wraith [53] describe a TDR dielectric tensiometer with a coaxial transmission line embedded in a porous material. Their ceramic has a stable structure which does not change with time like other sensors [54, 55]. Since ceramics tend to have a narrow pore size distribution, they used a number of ceramics with different pore sizes and integrated them into one sensor to extend the measurement range. The dielectric tensiometer principle [51] was used to design a new experimental prototype [64]. It used the MCM100-chip described in Sect. 13.2 to measure permittivity inside the ceramic. The aim of this work was to explore the design criteria for dielectric tensiometers based on porous media over the range from saturation to –60 kPa, which is suitable for automatic irrigation control applications. One of the major concerns was the effect of hysteresis.

The new prototype (see Fig. 13.17) used a ceramic (Coralith, grade C0) consisting of glass-bonded aluminum particles (Fairy Industrial Ceramics, Staffordshire, UK). It had a mean pore size of 11 μm, a porosity of 35%, and an air entry potential of –27 kPa. Three holes were drilled into this ceramic. The holes were slightly filled with electrically conducting silver-loaded epoxy glue (RS Components, Northants, UK) to prevent an air gap between the electrodes and the ceramic. Three stainless steel electrodes with a diameter of about 1 mm were carefully pushed into these holes. Finally the electrodes were soldered to an

electronic circuit board (see Fig. 13.4). Just above the ceramic a small air gap was kept to allow air to flow in and out the ceramic freely. This air gap is kept at atmospheric pressure by a tube with an outlet to the open air.

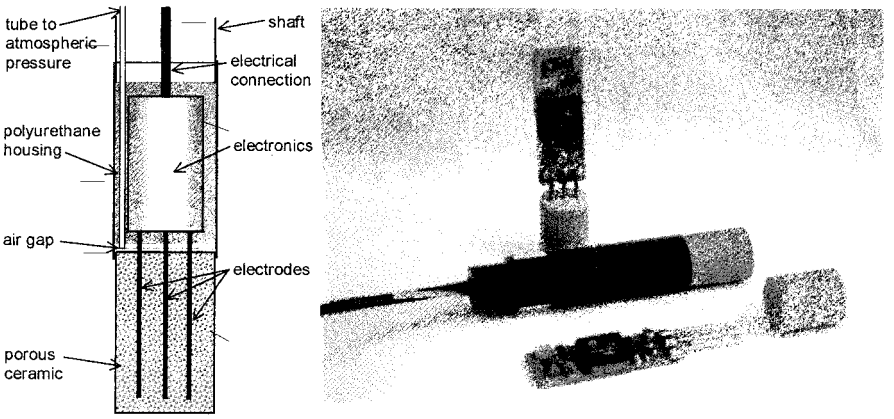

Fig. 13.17. A schematic drawing of a dielectric tensiometer (*left*), and a prototype with electronics, housing, and ceramic (*right*)

By using the FD method, small electrodes can be applied, contrary to similar TDR probes. The FD sensor, operating at 30 MHz, also measures conductivity, which might be a useful means to measure pore water salinity inside the ceramic. The electronics were embedded into a hard polyurethane molded cylinder of about 20 mm in diameter and a length of 5 cm. A flexible polyurethane output cable was connected to the electronics. The ceramic was 25 mm long and 19 mm in diameter. The complete sensor can be mounted on one end of a long tube, containing the cable and the air tube. In this way the dielectric tensiometer looks much like the hydraulic tensiometer, and it can be installed and removed from the soil very easily.

The FD sensor essentially measures the degree of saturation (S) of the ceramic, expressed as

$$S = \frac{\sqrt{\varepsilon} - \sqrt{\varepsilon_d}}{\sqrt{\varepsilon_s} - \sqrt{\varepsilon_d}}, \tag{13.9}$$

where ε is the dielectric permittivity in the ceramic in equilibrium with the surrounded soil and ε_d and ε_s are dielectric constants for the air-dry (d) and the water-saturated (s) ceramic. To find the relation between S and the soil matric potential (h) we use the inverted version of the van Genuchten equation [56], which is also used to characterize soil pf-curves:

$$h = \frac{1}{\alpha}\left[\left(\frac{S - S_r}{S_m - S_r}\right)^{-\frac{1}{m}} - 1\right]^{\frac{1}{n}}, \tag{13.10}$$

where S_m and S_r are the maximum and residual values of S, and α, m, and n are the shape parameters of the curve. To quantify these parameters for the ceramic used, its pf-curve was obtained from a drying curve cycle by using a conventional tension table. A sample of the ceramic was placed on the tension table immersed in silica paste. This sample was exposed to several matric potentials. Each time S was calculated from an oven-drying experiment. The curve found is in accordance with the model (see Fig. 13.18). This curve shows that the specific ceramic has an operating range that is suitable for irrigation management (–20 to –60 kPA). With parameter fitting the following van Genuchten parameters were found: $S_r = 0.111$; $S_m = 0.996$; $m = 0.405$; $n = 9.95$; and $\alpha = 0.041$.

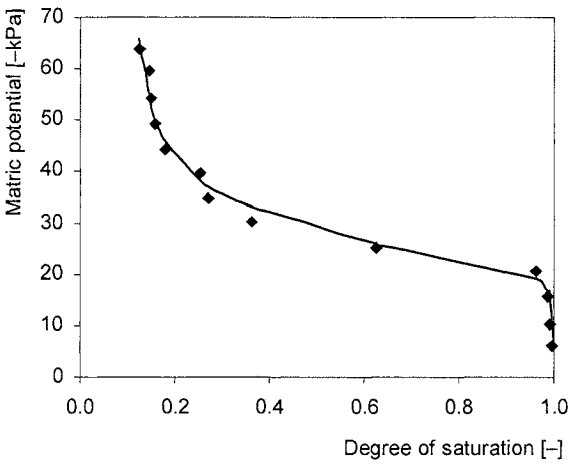

Fig. 13.18. pf-curve for the used ceramic with measured values during drying (♦) and fitted van Genuchten curve (—)

Thirteen prototype sensors were built. To observe the effect of drying and wetting, all 13 sensors were placed on a tension table in a saturated kaolin mixture. They were allowed to equilibrate at 0 kPa (saturation) for at least 2 days. The water potential of the tension table was controlled using a vacuum pump and the actual value was monitored using a hydraulic tensiometer. All measurements were carried out at a constant temperature of 20°C. Water potentials were decreased in small steps, typically –5 kPa. Values for each sensor were recorded following an equilibration period of 24 hours. This procedure was repeated until a water potential of –60 kPa was obtained. The water potential was then increased in small steps

until saturation (0 kPa) was reached. The results obtained from this experiment are shown in Fig. 13.19.

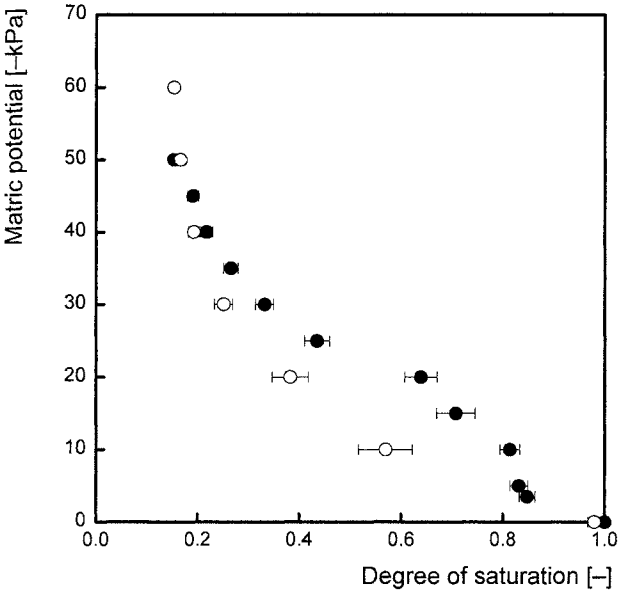

Fig. 13.19. Data obtained with 13 prototype sensors for the drying (•) and wetting (○) cycle. Horizontal lines indicate the standard error of the mean degree of saturation (Reproduced from Whalley et al. [64] with the permission of Blackwell Publishing)

The main wetting and drying curves clearly show hysteresis. We also see that for S between 0.2 and 0.8 these curves are flatter than the ceramic pf-curves found in the previous experiment. Furthermore, for S between 0.85 and 0.95 the behavior is also different. Because of this, the main drying curve alone is not suitable to obtain the matric potential. By not accounting for hysteresis effects, even by using a mean pf-curve, large errors up to ± 5 kPa may occur. When the sensor is not operated along the main drying or wetting curve an accurate value for h can never be obtained. Therefore it was decided to explore a hysteresis model that could correct for this effect in the area between the main wetting and drying curves.

Several hysteresis models are known [57, 58]. We have chosen the Kool and Parker model [59], which combines the empirical model of van Genuchten [56] for the moisture characteristic curve and the hysteresis model of Scott et al [60]. This model is capable of calculating matric potentials from the water content or saturation of the porous ceramic substrate, provided the wetting history is known. It requires that the main drying and wetting curves be known and expressed in terms of the van Genuchten equation (Eq. (13.10)). For all prototype sensors these

parameters were obtained by using a curve-fitting program. The results are shown in Table 13.6.

Table 13.6. Van Genuchten and dielectric parameters for 13 prototype dielectric tensiometers.

No.	S_r	S_m	α (d)* α (w)**	n (d) n (w)	m (d) m (w)	ε_r	ε_s
1	0.119	0.818	0.00371	3.356	1.784	7.5	31.9
			0.02018	205.0	0.007		
2	0.128	0.913	0.00038	1.961	117.48	9.4	35.3
			0.02147	74.6	0.027		
3	0.121	0.845	0.00395	4.035	1.065	10.3	36.9
			0.01715	32.96	0.371		
4	0.084	0.695	0.00673	5.690	0.436	7.8	30.9
			0.02003	741.3	0.003		
5	0.108	0.795	0.00493	4.481	0.674	10.0	36.2
			0.01423	8.395	0.153		
6	0.135	0.862	0.00411	4.935	0.879	8.1	30.5
			0.00609	2.400	1.114		
7	0.114	0.828	0.00429	4.536	0.740	4.3	27.0
			0.00669	2.495	0.798		
8	0.156	0.915	0.00380	4.718	1.065	4.8	26.4
			0.00245	2.157	3.692		
9	0.105	0.790	0.00506	18.88	0.134	4.4	27.5
			0.00585	2.876	0.745		
10	0.118	0.835	0.00510	6.299	0.391	4.7	27.4
			0.00685	2.764	0.709		
11	0.153	0.900	0.00500	6.720	0.431	4.7	26.9
			0.00507	2.542	1.101		
12	0.113	0.889	0.00541	12.57	0.149	4.8	25.1
			0.00645	2.901	0.574		
13	0.135	0.742	0.00411	3.837	0.938	4.7	31.2
			0.00454	2.380	1.237		

*(*d*) represents parameters determined from the drying cycle (0 to –60 kPa).
**(*w*) represents parameters determined from the wetting cycle (–60 to 0 kPa)

To test the hysteresis model, one prototype tensiometer (number 5) was exposed to a series of random changes in matric potential in the range 0 to –60 kPa. This was achieved by using a tension table. The sensor was immersed in wet silica paste together with a hydraulic tensiometer, which was used to monitor the matric potential of the silica paste. Both the drying pf-curve for the ceramic (see Fig. 13.18), as well as the Kool and Parker model using the van Genuchten parameters (Table 13.6, number 5), were used to obtain the matric potentials. Although the Kool and Parker model works unsatisfactorily at matric potentials lower than –30 kPa

(see Fig. 13.20, bottom), in general it behaves clearly better than the single drying pf-curve (see Fig. 13.20, top).

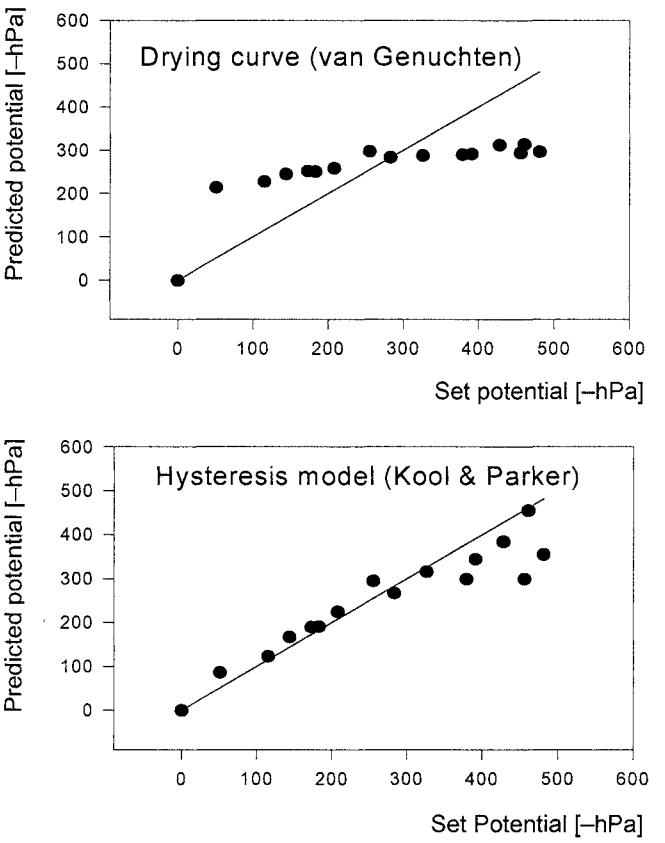

Fig. 13.20. Comparison between the output of a conventional tensiometer and a dielectric tensiometer by using the pf-curve for drying (*top*) and the Kool and Parker hysteresis model (*bottom*) (Reproduced from Whalley et al. [64] with the permission of Blackwell Publishing)

In the time series data plot (see Fig. 13.21) we see that the dielectric and hydraulic tensiometers show a similar shape. The time constant for both tensiometers seems to be in the same range, so they have a similar response time. Here also, in the dry range (–30 to –60 kPa), we see a discrepancy between the two types of tensiometers. In the wet range (0 to –30 kPa), both tensiometers have similar outputs. In general the Kool and Parker model gives more accurate results, but for longer

measuring periods and smaller matric potential differences we observed some drift in readings. This is due to the fact that the hysteresis model loses track of the historic data due to measuring errors. Fortunately the model synchronizes again after the tensiometer is brought back to (near) saturation or to the dry end of the curve. However, for practical irrigated crop production systems, where water is given more often, this is not the case. Here the differences in matric potentials will probably be so low that the hysteresis effect may be neglected and a mean pf-curve, somewhere between the wet and dry cycling curves, could be used instead.

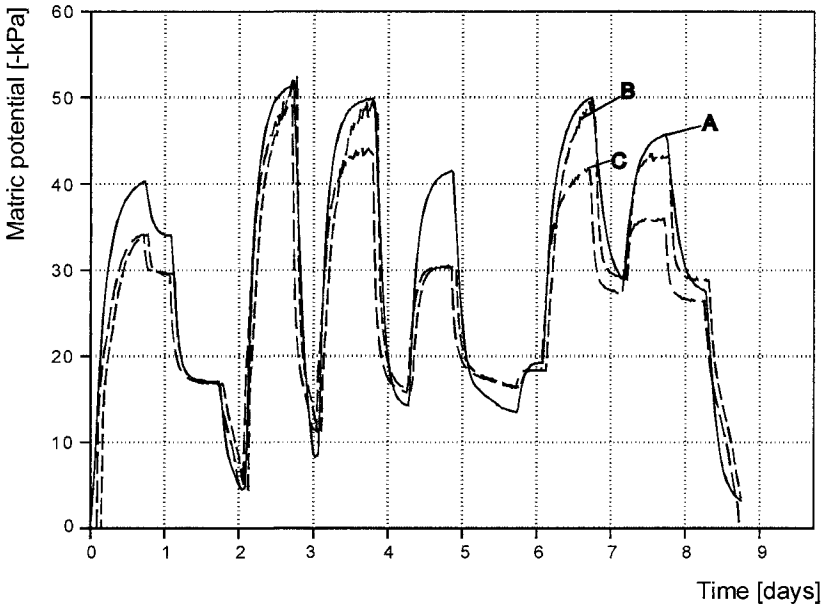

Fig. 13.21. Time series plot for the number 5 tensiometer. Readings from the hydraulic tensiometer (**A**) are compared with the calculated matric potential based on the Kool and Parker hysteresis model (**B**) and the drying pf-curve (**C**) (Reproduced from Whalley et al. [64] with the permission of Blackwell Publishing)

The development of our experimental tensiometer has raised a number of important issues that have general relevance to the class of matric potential sensors based on the use of porous materials. In particular the importance of air access into the porous material is relevant. The success of our experimental sensor, which was embedded in silica paste with much lower air entry potential, following the output of a tensiometer, demonstrates that the provision of access to air to invade the draining porous material is needed. An advantage of providing for air access into the ceramic is that it is then possible to install the sensors in the field in exactly the same way as a conventional tensiometer. Surrounding the sensor with

a paste with a very low air entry potential also has the advantage of providing a good connection between the soil and the sensor. We have shown that a model of hysteresis can be used to track changes in matric potential in a porous medium in equilibration with soil.

13.7 An FD Sensor Auto-Calibration Method for Volumetric Water Content

Monitoring soil water content (θ) with FD sensors that work in the lower RF range beneath 50 MHz involves a soil-specific calibration defined as $\theta = f(\varepsilon)$, similar to Eq. (13.5). In this frequency range a raised permittivity is found due to the Maxwell–Wagner effect. This effect is soil-texture dependent since it is influenced by the grain size of the soil particles. For clay this effect is larger than for sandy soils. For frequencies above 50 MHz this effect becomes smaller and can be neglected at even higher frequencies. Therefore dielectric soil-water content sensors that operate at frequencies above 100 MHz can generally do without a soil-specific calibration. Examples for this are the TDR sensors used by Topp [6, 17, 27] and the Theta probe (Delta-T Devices Ltd, Cambridge, UK) which is an FD sensor working at 100 MHz.

Generally, a gravimetric approach is used to calibrate these sensors. This is done by taking soil samples manually and measuring θ under wet and dry conditions while taking readings with the FD sensor (see Table 13.2 and Fig. 13.8). This method yields the most reliable calibration. However, under practical circumstances, soil texture and density have a large spatial variability. Inherently, FD sensors, when calibrated under laboratory conditions, exhibit in practice an error due to the local variation in soil texture and density. For this reason it would be nice to have an in situ calibration procedure for θ under practical conditions that could compensate for the Maxwell–Wagner rise automatically.

Little is found on this topic in the literature, but one paper reveals the fact that it might be possible to estimate the Maxwell–Wagner rise ($\Delta\varepsilon_{MW}$) by measuring ε at multiple, at least three, discrete frequencies in the range from 10 to 30 MHz [8, p 26]. Based on $\Delta\varepsilon_{MW}$ the more reliable permittivity at higher frequencies ($\varepsilon(f\rightarrow\infty)$) can be estimated. This idea is based upon the fact that soil water is either free or bound. Free water reacts with the electrical field at all frequencies up to its relaxation frequency, whereas bound water reacts better at lower frequencies. The Maxwell–Wagner rise in the dielectric spectrum at a specific measuring frequency is defined as:

$$\Delta\varepsilon_{MW}(f) = \varepsilon(f) - \varepsilon(f \rightarrow \infty), \tag{13.11}$$

where $\varepsilon(f)$ is the permittivity at the measuring frequency and $\varepsilon(f\rightarrow\infty)$ is the constant permittivity at a higher frequency where the Maxwell–Wagener effect can be neglected (e.g., 100 – 150 MHz). When $\varepsilon(f)$ is known at several measuring frequencies, $\varepsilon(f\rightarrow\infty)$ and $\Delta\varepsilon_{MW}(f)$ can be obtained through extrapolation toward a

higher frequency. Since FD and TDR sensors usually yield a more accurate result in this frequency range, the common Topp curve can than be used for calibration. In order to reduce this "bound water fault," here a simpler model is proposed to obtain an estimate for $\Delta\varepsilon_{MW}(f)$, based on taking an extra reading for ε at a slightly lower frequency (f^*) as can be seen in Fig. 13.22.

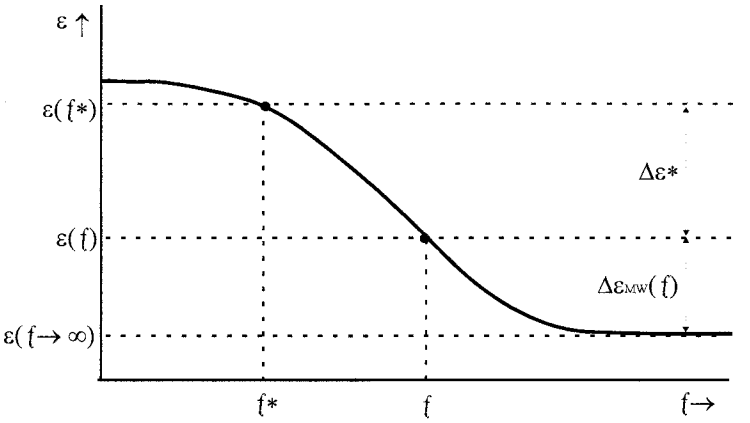

Fig. 13.22. Principle of automatic self-calibration based on estimation of the Maxwell–Wagner rise in the spectrum by taking readings for permittivity at two nearby frequencies

For this, it is assumed that $\Delta\varepsilon_{MW}(f)$ can be computed through a function F based on the difference in permittivity ($\Delta\varepsilon^*$) measured at two nearby frequencies f and f^* with $f^* < f$ defined as

$$\Delta\varepsilon^* = \varepsilon(f^*) - \varepsilon(f)\,, \tag{13.12}$$

and that this function F can be described as a Taylor polynomial:

$$\Delta\varepsilon_{MW}(f) = F(\Delta\varepsilon^*) \approx a_0 + a_1\Delta\varepsilon^* + a_2(\Delta\varepsilon^*)^2 + \ldots\,. \tag{13.13}$$

Next, $\varepsilon(f\to\infty)$ can then be obtained by using Eq. (13.11), and subsequently θ can be calculated from the standard Topp curve.

To explore this automatic soil-type calibration, some experiments were performed [61–63]. FD sensors were modified to measure permittivity at two frequencies (f = 10 and 20 MHz). This was achieved by successively switching two crystals to the microchip and taking readings with a PC. The sensors were used to measure ε, σ, and T inside five containers with a volume of 5 liters. Each container was filled with a different type of soil: sand, sandy loam, or loess all sampled from the field. For loess, three densities of which two were known (ρ_{pot4} = 1.1 g/cm³ and ρ_{pot5} = 1.4 g/cm³) were used. The samples were exposed to a constant temperature of 15°C, by using a water bath. They were wetted between air dry and field capacity ($\theta \approx$ 5–40%) in six or more steps for θ. The wetting water had low conductivity. For equilibration, after each wetting, three days were taken for the water to

redistribute. The values for water content were calculated from the amounts of wetting water. Due to inhomogeneous water distribution in the relatively huge pots, the readings obtained were not very accurate. For each sample, the permittivity was measured at the two frequencies. To show the Maxwell–Wagner rise, these values were plotted for a frequency of 20 MHz (see Fig. 13.23).

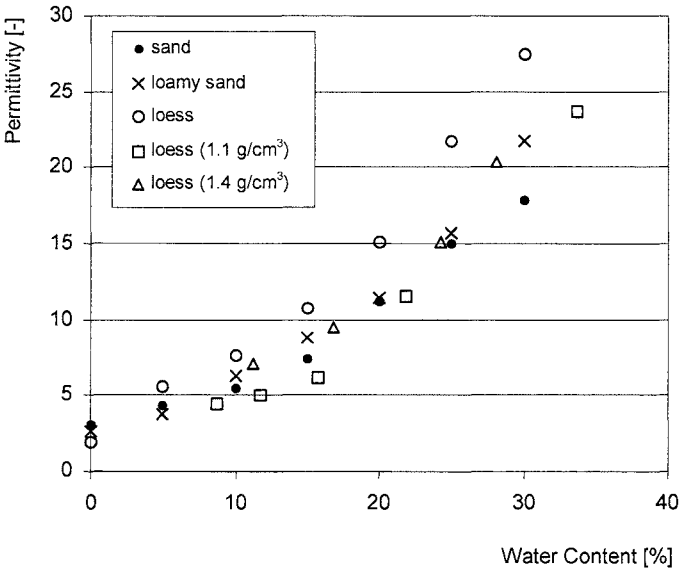

Fig. 13.23. Permittivity versus water content for three soil types (sand, loess, loamy sand) and for loess at two known densities (ρ_1 = 1.1 g/cm³ and ρ_2 = 1.4 g/cm³) taken with the FD sensors at a single frequency (20 MHz)

It can be seen that higher values for ε are found for loess (small soil particles) and that lower values are found for sand (large soil particles). Sandy loam shows a curve somewhere in between. This finding reflects nothing more than the fact that smaller particles provide a larger part of bound water and therefore a larger $\Delta\varepsilon_{MW}(f)$. Looking at the results for loess at two different densities (ρ_1 = 1.1 and ρ_2 = 1.4 g/cm³), we see that the Mawell–Wagner effect is larger at higher densities.

Next the 10 MHz readings from the FD sensors were also taken into account. The difference in permittivity ($\Delta\varepsilon^*$) was calculated for each reading based on Eq. (13.12). For each reading a value for $\varepsilon(f\rightarrow\infty)$ was obtained from the reference values for water content and the Topp curve. Then for each reading $\Delta\varepsilon_{MW}(f)$ was calculated by using Eq. (13.11). Now having a series of values for $\Delta\varepsilon_{MW}(f)$ and

$\Delta\varepsilon^*$ belonging together the function F and the coefficients a_i were obtained through a polynomial fitting program. By using this function for all readings, corrected values for θ were calculated. These corrected values, as well as θ results based on the Topp curve, are compared with the reference values for water content used in the experiment (see Fig. 13.24).

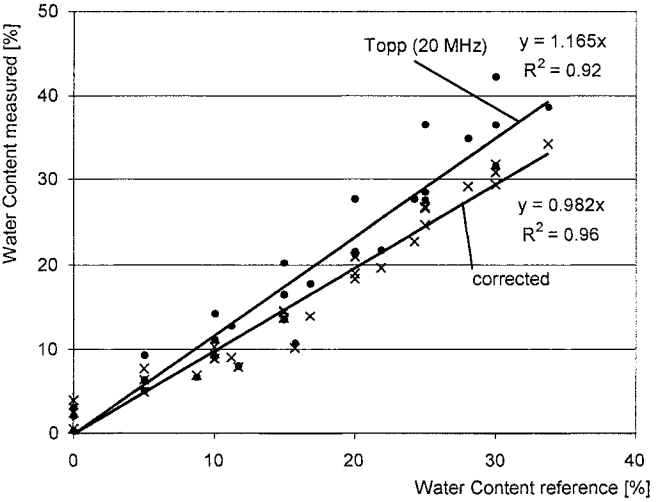

Fig. 13.24. Water content (θ) based on the auto-calibration algorithm (×) and water content based op the Topp curve applied at the 20 MHz permittivity data (•), compared to the reference water contents

It was shown that the correction scheme works fine for the used samples. The 1:1-line in Fig.13.24 for the auto-calibration values has a good correlation (R^2=0.96) and only deviates 2%. As expected, the Topp curve yields higher values since it is used on a low frequency of 20 MHz. It deviates 16.5% and has a lower correlation because of the soil-type dependency. Indeed, through a soil-specific calibration a better match than this 16.5% could have been obtained, but nevertheless this would as well lead to a higher spreading due to soil-type variation. It may be concluded that, by measuring at two frequencies, an interesting and important step toward self-calibration for soil type can be achieved. In practical circumstances, however, not only do soil type and density vary, but also temperature and conductivity have an influence on the dielectric spectrum. Hilhorst [8] showed that at higher conductivities the Maxwell–Wagner relaxation frequency shifts to the right. This suggests that the above relation is only valid at a specific conductivity or temperature. Further research is needed to explore these effects and to see whether the two-frequency approach will still work in practical situations, even after correction for temperature and conductivity.

Acknowledgment

The work presented in this chapter was mainly funded from the EC project WATERMAN (FAIR4-PL0681). We thank Wolfgang Paul from the Federal Agricultural Research Center, Institute of Technology and Biosystems Engineering, Braunschweig (Germany), for sharing his work on self-calibrating sensors from the WATERMAN project [65] with us. We are grateful to Kalman Rajkai from the Soil Science Department of the Research Institute for Soil Science and Agricultural Chemistry of Budapest (Hungary) for performing the water content calibration for our FD sensor and the willingness to share experimental data from the EC project QLK5-CT-1999-01349. Furthermore we have found Wim Stenfert Kroese from CONSENSOR b.v. (Rotterdam, the Netherlands) and Ton van Beek from Delft University (the Netherlands) willing to share their results from experiments performed with the concrete sensor, carried out in close collaboration with the Dutch Rijkswaterstaat. The work performed within our own laboratory at Wageningen-UR was co-funded by the Dutch DWK agricultural research program on Water and Nutrient Management. We also thank Max Wattimena, Henk van Roest, and Peter Nijenhuis for their work on the electronic design, software programming, and testing of the FD sensor. *Rockwool* is a trademark of Rockwool Grodan (Roermond, the Netherlands).

References

1. Debye P (1929) Polar molecules. Rheinhold, New York
2. Davidson DW, Cole RH (1951) Dielectric relaxation in glycerol, propylene glycol, and n-propanol. J Chem Phys 19:1481–1493
3. Stacheder M, Blume P, Fundinger R, Koehler K, Ruf R (2001) Reliability of Trime-TDR Sensors for moisture determination in pure and contaminated concrete. In: Proceedings of the fourth international conference on electromagnetic wave interactions with water and moist substances, Weimar, 13–16 May 2001, pp 266–273
4. Ferguson JG (1953) Classification of bridge methods of measuring impedances. Bell Syst Tech J 12:452–459
5. Hilhorst MA (1984) A sensor for the determination of the complex permittivity of materials as a measure for the moisture content. In Bergveld P (ed) Sensors & actuators. Kluwer Technical Books, Deventer, pp 79–84
6. Topp GC, Davis JL, Annan AP (1980) Electromagnetic determination of soil water content: measurements in coaxial transmission lines, Water Resour Res 16(3):574–582
7. Hilhorst MA, Groenwold J, De Groot JF (1992) Water content measurements in soil and rockwool substrates: dielectric sensors for automatic in situ measurements. In: Sensors in horticulture, Acta Hortic 304:209–218
8. Hilhorst MA (1998) Dielectric characterisation of soil. Doctoral-thesis, Wageningen University and Research Center, Wageningen, the Netherlands, ISBN 90-5485-810-9
9. Bratton WL, Pluimgraaff DJMH, Hilhorst MA (1995) CPT sensors for biocharacterization of contaminated sites. In: International symposium on cone penetration testing, Sweden, Oct

10. SOWACS website: www.sowacs.com, february 2004
11. Hadjar A (1997) Zerstörungsfreie Feuchtemessverfahren für Beton. In: Kupfer K (ed) 9 Feuchtetag, 7/18 Sept, MFPA an der Bauhaus-Universität Weimar, pp 301–316
12. van Beek A, Hilhorst MA (1999) Dielectric characterization of young concrete. Heron 44(1), pp 3–17
13. Sokoll T, Jannsen B, Jacob AF (2002) A novel sensor for measuring ion concentration in concrete structures. In: Kupfer K (ed) 11 Feuchtetag, 18/19 Sept 2002, pp 36–46
14. Foster KR, Schwan HP (1986) Dielectric permittivity and electrical conductivity of biological materials. In: Polk C, Postow E (eds) Handbook of biological effects of electromagnetic fields. CRC Press, Boca Raton, FL, pp 27–98
15. Nacke T, Frense D, Göller A, Beckmann D (2001) Impedance spectroscopy – a tool for in situ biomass analyses and for the study of the toxic sensitivity of cells in suspension cultures. In: Proceedings of the fourth international conference on electromagnetic wave interactions with water and moist substances, Weimar, 13–16 May 2001, pp 93–100
16. Hilhorst MA, Balendonck J, Kampers FWH (1993) A broad-bandwidth mixed analog/digital integrated circuit for the measurement of complex impedances. IEEE J Solid-state Circuits 28(7):764–769
17. Topp GC, Davis JL, Annan AP (1982) Electromagnetic determination of soil water content using TDR: II. Evaluation of installation and configuration of parallel transmission lines. Soil Sci Soc Am J 46:678–684
18. Hilhorst MA, Dirksen C (1994) Dielectric water content sensors: time domain versus frequency domain. In: Proc of the symposium on TDR in environmental, infrastructure and mining applications, Evanston, Illinois, Sept 1994, pp 23–33
19. Dirksen C, Hilhorst MA (1994) Calibration of a new frequency domain sensor for soil water content and bulk electrical conductivity. In: Proceedings of the symposium on TDR in environmental, infrastructure and mining applications, Evanston, Illinois, Sept 1994, pp 43–153
20. Balendonck J (1997) Smart sensor chip for dielectric measurements In: Proceedings 8th international congress, transducers & systems, Sensor 97, Nürnberg, May 1997, vol 1, pp 253–258
21. Balendonck J, Hilhorst MA (1998) MCM100 Smart sensor interface for complex impedance measurement. Datasheet and application note. Report IMAG-DLO, Wageningen, Note P98–50, 45 pp
22. Balendonck J, Hilhorst MA (2001) Application of an intelligent dielectric sensor for soil water content, electrical conductivity and temperature. In: Proceedings of the 18th IEEE instrumentation and measurement technology conference, IMTC-2001, Budapest, 23–25 May 2001, pp 1817–1822
23. Seyfried MS, Murdock MD (2002) Effects of soil type and temperature on soil water measurement using a soil dielectric sensor. In: I.C. Paltineau (ed.), First International Symposium on Soil Water Measurement using Capacitance and Impedance, Beltsville, MD. 6–8 November 2002, pp 1–13
24. Kaatze U, Uhlendorf V (1981) The dielectric properties of water at microwave frequencies. Z Phys Chem, Neue Folge, 126:151–165
25. Balendonck J, Hilhorst MA (2001) WET sensor application note. IMAG Report 2001-07, Wageningen
26. Heimovaara TJ (1993) Time domain reflectometry in soil science: theoretical backgrounds, measurements and models. PhD thesis, University of Amsterdam

27. Topp GC, Ferré PA (2001) Electromagnetic wave measurements of soil water content: a state-of-the-art. In: Fourth international conference on electromagnetic wave interaction with water and moist substances, Weimar, 13–16 May 2001
28. Kuyper MC, Balendonck J (1997) Application of dielectric soil moisture sensors for real-time automated irrigation control. In: Sensors in horticulture, Tiberias, Israel, August 1997
29. Perdok UD, Kroesbergen B, Hilhorst MA (1996) Influence of gravimetric water content and bulk density on the dielectric properties of soil. Eur J Soil Sci 47:367–371
30. Kalman Rajkai (2002) Personal communication, Soil Science Department of the Research Institute for Soil Science and Agricultural Chemistry of Budapest, Hungary
31. Sonneveld C, van den Ende J (1971) Soil analysis by means of a 1:2 volume extract. Plant Soil 35:505–516
32. Hilhorst MA, Balendonck J (1999) A pore water conductivity sensor to facilitate non-invasive soil water content measurements. In: Staffort JV (ed) Proceedings of the 2nd European conference in precision agriculture, Society of Chemical Industry, Odense, pp 211–220
33. Hilhorst MA (2000) A pore water conductivity sensor. Soil Sci Soc Am J 64(6), pp 1922–1925
34. Dirksen C, Dasberg S (1993) Improved calibration of time domain reflectometry for soil water content measurements. Soil Sci Soc Am J 57:660–667
35. Balendonck J, Hilhorst MA, van Roest H (2002) Water content and temperature dependency of pore water conductivity for the FD sensor in growing substrates. In: 11 Feuchtetag, 18/19 Sept 2002, MFPA an der Bauhaus-Universität Weimar, pp 67–76
36. van Beek A (2000) Dielectric properties of young concrete, non-destructive dielectric sensor for monitoring the strength development of young concrete. Dissertation, Delft University
37. NEN 5970 (1999) Bepaling van de druksterkteontwikkeling van jong beton op basis van de gewogen rijpheid, oktober
38. ASTM C-1074-93 (1998) Revised standard for testing young concrete, defined by the Am Soc for Testing and Materials
39. Tobio JM (1957) A study of the setting process: dielectric behaviour of several Spanish cements. In: Silicates Industrials, Comunication présentée aux Journées Internationales d'études, Liant hydrauliques 1957, de l'Assoiation belge pour favoriser L'étude des Verres et Composés siliceux, pp 30–35, 81–87
40. De Loor GP (1953) Method of obtaining information on the internal dielectric constant of mixtures. Appl Sci Res pp 479–482
41. Al-Qadi IL, Hazim OA, Su W, Riad SM (1995) Dielectric properties of Portland cement concrete at low frequencies. J Mat Civ Eng 7:192–198
42. van Breugel K, Hilhorst MA, van Beek K, Stenfert-Kroese W (1996) In situ measurement of dielectric properties of hardening concrete as a basis for strength development. In: Proceedings of the 3rd conference on non-destructive evaluation of civil structures and materials, Sept 1996, pp 7–21
43. Hilhorst MA, van Breugel K, Pluimgraaf DJMH, Stenfert Kroese W (1996) Dielectric sensors used in environmental and construction engineering. Mat Res Soc Symp Proc 411:404–406
44. Stenfert Kroese WH, Hilhorst MA (2000) Method for determining the degree of hardening of a material. Patent WO9642014 and US 6023170, 2 Aug 2000

45. Dirksen C (1999) Soil Physics Measurements. Geo-Ecology, Catena Verlag, Reiskirchen, Germany, 1999
46. Richards LA (1949) Methods for measuring soil moisture tension. Soil Sci 68:95–112
47. Mullins CE, Mandiringana OT, Nisbet TR, Aitken MN (1986) The design, limitations, and use of a portable tensiometer. J Soil Sci 37:691–700
48. Bouyoucos GJ, Mick AH (1940) Electrical resistance method for the continuous measurement of soil moisture under field conditions. Michigan Agricultural Experimental Station, Tech Bull no 172
49. Thomson SJ, Armstrong CF (1987) Calibration of the Watermark Model 200 Soil Moisture Sensor. Appl Eng Agric 3(2):186–189
50. Spaans EJA, Baker JM (1992) Calibration of the Watermark soil-water sensors for soil matric potential and temperature. Plant Soil 143:213–217
51. Hilhorst MA, de Jong JJ (1988) A dielectric tensiometer. Agricultural Water Management 13:411-415, technical note
52. Liu Jin-Chen (2002) Ein neues Verfahren zur Messung des Matrixpotenzials im Bodem. In: 11 Feuchtetag, 18/19 Sept 2002, MFPA an der Bauhaus-Universität Weimar, pp 77–84
53. Or D, Wraith JM (1999) A new soil matric-potential sensor based on time-domain-reflectometry. Water Resour Res 35:3399–3407
54. Bouyoucos GJ (1953) More durable plaster of Paris blocks. Soil Sci 76:447–451
55. Liu Jin-Chen (1999) Device and method for determining properties of a soil. US Patent 5.898.310, 27 Apr 1999
56. van Genuchten MT (1980) A closed-form equation for predicting the hydraulic conductivity of unsaturated soils. Soil Sci Soc Am J 44:892–898
57. Jaynes DB (1984) Comparisons of soil-water hysteresis models. J Hydrol 75:289–299
58. Otten W, Raats PAC, Kabat P (1999) Hydraulic properties of root-zone substrates used in greenhouse horticulture. In: MTh van Genuchten et al (eds) Characterization and measurement of the hydraulic properties of unsaturated media, proceedings of international workshop, 22–27 Oct 1997, Riverside, California, pp 477–489
59. Kool JB, Parker JC (1987) Development and evaluation of closed form expressions for hysteretic soil hydraulic properties. Water Resour Res 23:105–114
60. Scott PS, Farquhar GJ, Kouwen N (1983) Hysteretic effects on net infiltration. In: Advances in infiltration, Publication 11–83, American Society of Agricultural Engineering, St. Joseph, MI, pp 163–170
61. Paul W, Hilhorst MA, Münstermann C, Schmitz M (1998) Neue Meßtechniken zur gleichzeitigen Bestimmung von Wassergehalt, Wasserspannung und verfügbaren Düngersalzen im Boden, Vortrag Internationale Tagung Landtechnik, Garching 1998, VDI-MEG Verlag, Düsseldorf, 1998, S.223–228
62. Balendonck J et al (2001) Waterman. Final report, EC-project FAIR1–CT95–0681, CD-ROM, 13 Jan 2001
63. Paul W (2002) Prospects for controlled application of water and fertiliser, based on sensing permittivity of soil. Comput Electron Agric 36:51–163
64. Whalley WR, Watts CW, Hilhorst MA, Bird NRA, Balendonck J, Longstaff DJ (2001) The design of porous material sensors to measure the matric potential of water in soil. Eur J Soil Sci 52:511–519
65. Paul W (1998) Sensors for soil attributes, plant transpiration and water stress. In: Int Conf on Agr Eng; part 2, Oslo 1998, 98-C-010, pp 850–853

Measurement Methods and Sensors in Time Domain